Published in final edited form as:
Neuron. 2009 December 24; 64(6): 807–827. doi:10.1016/j.neuron.2009.11.006.

Leucine-Rich Repeat Kinase 2 Regulates the Progression of Neuropathology Induced by Parkinson's Disease-related Mutant α-synuclein

Xian Lin[1,^], **Loukia Parisiadou**[1,^], **Xing-Long Gu**[1,^], **Lizhen Wang**[1,^], **Hoon Shim**[1,#], **Lixin Sun**[1], **Chengsong Xie**[1], **Cai-Xia Long**[1], **Wan-Jou Yang**[1], **Jinhui Ding**[2], **Zsu Zsu Chen**[3], **Paul E. Gallant**[4], **Jung-Hwa Tao-Cheng**[5], **Gay Rudow**[6], **Juan C. Troncoso**[6], **Zhihua Liu**[7], **Zheng Li**[8], and **Huaibin Cai**[1,*]

[1]Units of Transgenesis, Laboratory of Neurogenetics, National Institute on Aging, National Institute of Mental Health, National Institutes of Health, Bethesda, MD 20892

[2]Bioinformatics Core, Laboratory of Neurogenetics, National Institute on Aging, National Institute of Mental Health, National Institutes of Health, Bethesda, MD 20892

[3]Department of Biology, University of Alabama at Birmingham, AL 35233

[4]Laboratory of Neurobiology, National Institute of Neurological Disorders and Stroke, National Institute of Mental Health, National Institutes of Health, Bethesda, MD 20892

[5]EM Facility, National Institute of Neurological Disorders and Stroke, National Institute of Mental Health, National Institutes of Health, Bethesda, MD 20892

[6]Division of Neuropathology, Department of Pathology, The Johns Hopkins University School of Medicine, Baltimore, MD 21205

[7]Laboratory of Immunology, National Institute of Allergy and Infectious Diseases, National Institute of Mental Health, National Institutes of Health, Bethesda, MD 20892

[8]Unit on Synapse Development and Plasticity, Genes, Cognition and Psychosis Program, National Institute of Mental Health, National Institutes of Health, Bethesda, MD 20892

Summary

Mutations in α-*synuclein* and *Leucine-rich repeat kinase 2* (*LRRK2*) are linked to autosomal dominant forms of Parkinson's disease (PD). However, little is known about any potential pathophysiological interplay between these two PD-related genes. Here we show in transgenic mice that although over-expression of *LRRK2* alone did not cause neurodegeneration, the presence of excess *LRRK2* greatly accelerated the progression of neuropathological abnormalities developed in PD-related A53T α-*synuclein* transgenic mice. Moreover, we found that LRRK2 promoted the abnormal aggregation and somatic accumulation of α-synuclein in A53T mice, likely resulted from the impairment of

*Corresponding author: Unit of Transgenesis, Laboratory of Neurogenetics, National Institute on Aging, National Institutes of Health, Building 35, Room 1A116, MSC 3707, 35 Convent Drive, Bethesda, MD 20892-3707. Phone: 301-402-8087; Fax: 301-480-2830; caih@mail.nih.gov.
^The first four authors should be regarded as joint First Authors.
#Current address: School of Medicine at Virginia Commonwealth University, Richmond, VA 23298.

Conflict of interest statement: There is no competing financial interest of all researchers involved in this work.

microtubule dynamics, Golgi organization, and ubiquitin-proteasome pathway. Conversely, genetic ablation of *LRRK2* preserved the Golgi structure, suppressed the aggregation and somatic accumulation of α-synuclein, and thereby delayed the progression of neuropathology in A53T mice. These findings demonstrate that over-expression of *LRRK2* enhances α-synuclein-mediated cytotoxicity and suggest inhibition of *LRRK2* expression as a potential therapeutic option for ameliorating α-synuclein-induced neurodegeneration.

Keywords

LRRK2; G2019S; α-synuclein; A53T; Golgi apparatus; microtubule; ubiquitin; mitochondria; aggregation; transgenic; knockout; Parkinson's disease

Introduction

Parkinson's disease (PD) is characterized pathologically by relatively selective loss of midbrain and brain stem catecholaminergic neurons and by deposition of α-synuclein (α-syn) aggregates in cell bodies and nerves (Nussbaum and Polymeropoulos, 1997). Since mutations in both α-*syn* and *Leucine-rich repeat kinase 2* (*LRRK2*) cause familial forms of PD that resemble sporadic PD pathologically (Hardy et al., 2006), these genetic mutations provide valuable molecular tools to study the pathogenesis of PD. The etiology of PD remains elusive; however, it has been generally accepted that the formation of α-syn aggregates is a key step in the pathogenesis of PD (Trojanowski et al., 1998).

Mutations in the α-*syn* gene, including missense mutations (A53T and A30P) and gene duplication/triplication, lead to the development of early-onset familial PD (Hardy et al., 2006). Furthermore, α-syn is a main component of abnormal intracellular deposits known as Lewy bodies (LB) and Lewy neurites (LN) found in PD brains (Spillantini et al., 1997). While both wild-type (WT) and mutant α-syn form fibrillar aggregates, PD-related α-syn mutations greatly accelerate the formation of fibrils as compared to WT protein (Conway et al., 1998;Narhi et al., 1999). α-syn aggregates cause various cytotoxicity, including impairment of proteasomal and lysosomal activities, disruption of ER-Golgi traffic and microtubule-based transport, and dysfunction of mitochondria (Cooper et al., 2006;Cuervo et al., 2004;Gosavi et al., 2002;Lee et al., 2006;Tanaka et al., 2001). Because α-syn aggregates are detrimental to cells, many studies on PD therapy are focused on identifying elements that affect α-syn's ability to form aggregates and fibrils (Savitt et al., 2006).

Mutations in *LRRK2* have been linked to both familial and sporadic forms of PD (Paisan-Ruiz et al., 2004;Zabetian et al., 2005;Zimprich et al., 2004). LRRK2 protein, also known as Dardarin, contains multiple functional domains and may function as both an active GTPase and kinase (Li et al., 2007;West et al., 2005). The most common mutation of *LRRK2* is the G2019S substitution at the conserved Mg^{++}-binding motif within the kinase domain (Gilks et al., 2005;Nichols et al., 2005), which may increase the putative LRRK2 kinase activity (West et al., 2005). PD-related missense mutations are also found within the GTPase domain of LRRK2 (Paisan-Ruiz et al., 2004;Zimprich et al., 2004), which has been shown to physically interact with both α and β tubulin and may regulate the dynamics of microtubules in neurons (Gandhi et al., 2008;Gillardon, 2009). Although mutant LRRK2 is toxic when over-expressed in cultured cells (Greggio et al., 2006;Smith et al., 2006) and *Drosophila* (Imai et al., 2008;Liu et al., 2008), no apparent neuronal loss is observed in transgenic mice over-expressing PD-related *LRRK2* R1441G and R144C mutants (Li et al., 2009;Tong et al., 2009). The pathogenic mechanism of PD-related *LRRK2* mutants remains obscure.

To study the function of LRRK2 and how mutant LRRK2 causes neuron degeneration *in vivo*, we have generated *LRRK2* knockout (*LRRK2*$^{-/-}$) and transgenic mice expressing human WT, G2019S, or kinase domain-deletion *LRRK2*. Neither deletion nor over-expression of *LRRK2* caused any overt gross neuropathological abnormalities in mutant mice. However, co-expression of WT, G2019S, or kinase domain-deletion *LRRK2* with the PD-related A53T α-*syn* caused synergistic toxicity to neurons that accelerated the progression of α-syn-mediated neuropathology. Conversely, inhibition of *LRRK2* expression reduced the aggregation and somatic accumulation of α-syn, and delayed the progression of α-syn-mediated neuropathology. Our findings suggest that LRRK2 may regulates A53T α-synuclein-mediated neuropathology through modulating the intracellular trafficking and accumulation of α-syn.

Results

Generation of *LRRK2* and α-*synuclein* inducible transgenic mice

As described previously (Wang et al., 2008), we have generated *LRRK2* inducible transgenic mice in which the expression of carboxyl-terminal hemagglutinin (HA)-tagged human wild-type (WT), G2019S, or kinase-deletion (KD) mutant *LRRK2* was under the transcriptional control of tetracycline operator (*tetO*) (Figure 1A). To make the *KD* expression construct, we deleted residues from 1887 to 2102 of LRRK2, resulting in a complete deletion of its kinase domain. In parallel with the generation of *LRRK2* inducible transgenic mice, we also used the same strategy to generate new lines of human α-*synuclein* (α-*syn*) A53T inducible transgenic mice (*tetO-A53T*). Given the expression pattern of *LRRK2* (Galter et al., 2006) is similar to that of *calcium/calmodulin-dependent protein kinase II-alpha* (*CaMKII*) in the brain, we crossbred *tetO-LRRK2* and *tetO-A53T* mice with a line of *CaMKII* promoter-controlled tetracycline transactivator (tTA) (*CaMKII-tTA*) mice (Mayford et al., 1996) to achieve high level expression of *LRRK2* or α-*syn* in the forebrain regions. Accordingly, our previous *in situ* hybridization experiments showed that the expression of human *LRRK2* was mainly detected at the olfactory bulb, cerebral cortex, hippocampus and striatum in the brain of *tetO-LRRK2* and *CaMKII-tTA* double transgenic mice (Wang et al., 2008). For simplicity, we will later refer to the *tetO-LRRK2* and *CaMKII-tTA* double transgenic mice as *LRRK2WT*, *G2019S*, and *KD* transgenic mice, respectively. We generated five independent lines of *LRRK2WT*, three independent lines of *G2019S*, and three independent lines of *KD* transgenic mice. We refer to the E3 line as the *G2019S* transgenic mice and the C74 line as the *LRRK2* WT expression line (*LRRK2WT*) in later studies. In both *G2019S* and *LRRKWT* mice, the expression of LRRK2 protein was increased by about 8 to 16-fold compared to the endogenous one (Figure 1B, Supplemental Figure S1B). Additionally, we designate line C77 as the *LRRK2* WT low expression line (*LRRK2WT-L*) and line D10 as the *KD* mice. In the brain homogenate of *KD* mice, a doublet of LRRK2-positive bands was detected in which the lower one likely represents the exogenous human LRRK2 with truncated kinase domain (Figure 1B). The expression level of exogenous human LRRK2 between *LRRK2WT-L* and *KD* transgenic mice was comparable, which was about 8 to 16-fold less than that of *LRRK2WT* mice (Supplemental Figure S1C). Therefore, the expression of LRRK2 was only modestly increased (< 1-fold) in the brain of *LRRK2WT-L* and *KD* mice as compared to *nTg* controls (Figure 1B). Q-RT-PCR was used to quantify the expression of exogenous *LRRK2* in the brain of *LRRK2WT-L* and *KD* mice. The transcription of exogenous *LRRK2* mRNA was about 5 and 15-fold increase in the brain of *LRRK2WT-L* and *KD* mice as compared to *nTg* controls (Supplemental Figure S1D). The rather lower accumulation of exogenous LRRK2 protein in the *KD* mouse brain may likely reflect the instability of this mutant protein.

Under the same transcriptional activation of *CaMKII* promoter-controlled tTA, the expression pattern of human α-*syn* was the same as that of *LRRK2* transgene in the brain (Figure 1C, upper panel). Administration of doxycycline (DOX) suppressed the expression of exogenous α-syn

in this "tet-off" system (Figure 1C, middle panel). The expression level of human A53T α-syn protein was increased by about 30-fold as compared to endogenous protein (Figure 1D, Supplemental Figure S1B). Noticeably, under the *CaMKII* promoter only a small fraction (<5%) of midbrain DA neurons expressed the transgene (Supplemental Figures. S1E–G). Therefore, we focus our studies on the cortex and striatum where the exogenous α-syn and LRRK2 are widely expressed.

G2019S inducible transgenic mice developed similar locomotor abnormalities as *A53T* transgenic mice

All lines of *LRRK2WT, G2019S*, and *KD* transgenic mice were viable and developed normally. *G2019S* mice appeared to gain less body weight compared to non-transgenic (*nTg*) and *tetO-G2019S* single transgenic mice starting at 12 months of age (Supplemental Figure S2A, $p < 0.0001$). However, no significant difference in body weight was found between *G2019S* and *CaMKII-tTA* mice (Supplemental Figure S2A). The motor functions of *G2019S* mice were examined by Rotarod and Open-field tests. *G2019S* mice performed normally in the Rotarod test (Supplemental Figure S2C). However, they displayed significantly increased ambulatory activities starting at 12 months of age (Figure 1E, $p < 0.05$). G2019S mice also showed a trend of increased rearing activities, but it did not reach the statistic significance (Figure 1G). In addition, there were no apparent motor phenotypes detected in *LRRK2WT* mice up to 6 months of age (Supplemental Figure S2F–H). By contrast, *A53T* transgenic mice weighted significantly less starting at 4 months of age (Supplemental Figure S2B, $p < 0.0005$), and began to display drastic increases of ambulatory activities at 2 months of age (Figure 1F, $p < 0.0001$) and elevated rearing activities at 6 months of age (Figure 1H, $p < 0.05$). Together, the motor behavioral studies suggest that over-expression of G2019S *LRRK2* and A53T α-*syn* in the forebrain regions may induce a similar damage to the neural circuitry responsible for regulating motor activities.

A53T inducible transgenic mice developed progressive neuropathological abnormalities compared to *G2019S* transgenic mice

To determine if any neuropathological abnormalities developed in *A53T* and *G2019S* transgenic mice, we examined the brain sections of mutant and control animals for neurodegeneration and associated astrocytosis and microgliosis. The neurodegeneration was revealed by Jade C and cleaved-caspase 3 staining. The presence of reactive astrocytes was examined by staining for glial fibrillary acidic protein (GFAP). The morphology of microglia was visualized by staining for ionized calcium binding adaptor molecule-1 (Iba1). Both Jade C and c-caspase 3 staining were negative in the brain sections derived from 20-month old *G2019S* transgenic mice (Figures 2Ad, 2Bd; Table 1). Consistently, stereological studies revealed no significant changes in neuron counts at both the frontal cortex and dorsal striatum between *G2019S* and age-matched *nTg* mice (Figure 2E–G). In addition, no apparent increase of reactive astrocytosis or microglial activation was observed in the striatum and cortex of *G2019S* transgenic mice as compared to control *nTg* animals (Figure 2; Table 1 and Table 2). Similarly, no obvious gross neuropathological phenotypes were found in 12-month old *LRRK2WT* transgenic mice (Table 1, Supplemental Figures S2I–L).

No apparent neuropathological abnormalities were detected in the striatum of 3-month old A53T mice (Figures 2Aa–2Da). Such neuropathology became obvious when *A53T* transgenic mice were examined at 12 and 20 months of age (Figure 2; Table 1 and Table 2). Widespread neurodegeneration was evident in the brains of 20-month old *A53T* transgenic mice (Figures 2Ac–2Bc, 2E). Massive neuronal loss in the frontal cortex (>80%) and dorsal striatum (>74%) of *A53T* mice was estimated by unbiased stereological approaches (Figures 2F–G). Therefore, *A53T* mice developed age-dependent, progressive neruodegeneration; whereas, *G2019S* mice did not show any obvious gross neuropathological phenotypes.

LRRK2 accelerated the progression of A53T α-syn-mediated neuropathology

To test whether over-expression of *LRRK2* affects A53T α-syn-mediated neurodegeneration, we generated *A53T/LRRK2WT-L, A53T/LRRK2WT, A53T/G2019S* and *A53T/KD* double transgenic mice and examined the progression of neuropathological alterations (Figure 3). Compared to 1-month old *A53T* single transgenic mice, the number of GFAP-positive astrocytes was significantly elevated in the striatum of age-matched *A53T/LRRK2WT-L* and *A53T/LRRK2WT* double transgenic mice (Figures 3A, 3E). In addition, more GFAP-positive astrocytes were found in the brain of *A53T/LRRK2WT* mice than *A53T/LRRK2WT-L* mice (Figures 3A, 3E), suggesting that the expression level of *LRRK2* influences the progression of α-syn-mediated neuropathology. A similar increase of microglial activation was also observed in *A53T/LRRK2WT-L* and *A53T/LRRK2WT* double transgenic mice (Figures 3B, Table 2). Besides gliosis, neurodegeneration was also accelerated in the striatum of *A53T/LRRK2WT-L* and *A53T/LRRK2WT* transgenic mice (Figure 3, Table 1). Co-staining of caspase 3 with Ctip2, a specific marker for striatal medium-size spiny neurons (MSN) (Arlotta et al., 2008), revealed that most of these degenerating neurons were MSNs (Supplemental Figure S3). The prevalence of neurodegeneration in *A53T/LRRK2WT* double transgenic mice was also elevated in a *LRRK2* dose-dependent fashion (Figure 3F, Table 1). Taken together, these findings demonstrate that over-expression of *LRRK2* accelerates the progression of α-syn-mediated neuropathology.

Since the G2019S mutation in *LRRK2* causes late onset PD, we decided to investigate whether the G2019S mutation would further enhance the neuropathology in *A53T/G2019S* mice as compared to *A53T/LRRK2WT* double transgenic mice. A significant exacerbation of astrocytosis, microgliosis, and neurodegeneration was observed in the striatum of *A53T/G2019S* mice as compared with age-matched *A53T* single transgenic animals (Figure 3; Table 1 and Table 2). When we compared the pathological phenotypes of 1-month old *A53T/LRRK2WT* and *A53T/G2019S* mice, we found the number of Jade C-positive and GFAP-positive cells, and the activation of microglia were significantly increased in the striatum of *A53T/G2019S* mice as compared to *A53T/LRRK2WT* animals ($p < 0.0001$, 0.005, and 0.002, respectively; Figure 3E; Table 1 and Table 2). However, when we compared the numbers of neurons remained in the striatum of *A53T/LRRK2WT* and *A53T/G2019S* mice, the difference was not statistically significant ($p = 0.14$, Figure 3F). To further investigate whether the kinase domain of LRRK2 is critical in regulating α-syn A53T-mediated neuropathology, we compared the progression of neuropathology between *A53T/KD* and *A53T/LRRK2WT-L* transgenic mice. As shown in Figure 3, the presence of kinase-deletion *LRRK2* also accelerated A53T-mediated neuropathology to a similar extent as *LRRK2WT-L* (Figure 3 and Table 1–Table 2). These data suggest that the kinase domain of LRRK2 perhaps is not critical in modulating *A53T*-induced neuropathological abnormalities.

We further examined the neurodegeneration of *A53T, A53T/LRRK2WT*, and *A53T/G2019S* mice at 6 months of age (Figures 3G–H). While no obvious neuronal loss was observed in both *LRRK2WT* and *G2019S* mice, a significant reduction (30%) of striatal neurons was found in *A53T* single transgenic mice (Figures 3G–H, $p < 0.02$). More dramatic neuronal loss was detected in the dorsal striatum of *A53T/LRRK2WT* (80%) and *A53T/G2019S* (85%) mice (Figures 3G–H, $p < 0.001$ and 0.0001). However, the numbers of residual neurons in the dorsal striatum of *A53T/LRRK2WT* and *A53T/G2019S* mice were not statistically different ($p = 0.45$, Figure 3H). These observations from adult mice further support our earlier findings that the presence of excess WT and G2019S *LRRK2* exacerbates A53T-mediated neurodegeneration and the expression level of LRRK2 rather the PD-related G2019S mutation perhaps is more important in accelerating A53T α-*syn*-mediated pathogenesis.

With the concern whether over-expression of any exogenous protein could accelerate α-*syn*-mediated neuropathology, we crossbred *A53T* mice with a line of green fluorescent protein

(GFP) transgenic mice that selectively express GFP in striatal neurons (Gong et al., 2003). We did not observe any significant influence of GFP on the progression of neuropathology in *A53T/GFP* double transgenic mice (Figure 3E, Supplemental Figure S4). In addition, to test if *LRRK2* selectively potentiates A53T-mediated neuropathology, we crossbred *G2019S* mice with *amyloid precursor protein* (*APP*) inducible transgenic mice in which an Alzheimer's disease-related double mutant version of chimeric mouse/human APP is over-expressed 10 to 30-fold compared to the endogenous APP (Jankowsky et al., 2005). We found that *LRRK2* did not accelerate *APP*-mediated astrocytosis and microgliosis in *APP/G2019S* double transgenic mice (Supplemental Figure S5). Together, these observations support a specific effect of *LRRK2* on the pathogenesis of α-*syn* A53T mutation.

LRRK2 promoted the abnormal accumulation of α-syn in cell bodies

The α-syn staining is normally confined to axon terminals (Maroteaux et al., 1988), which was shown here as small puncta in the coronal striatal sections of 3-month old *A53T* mice and 20-month old *nTg* mice (Figure 4). Interestingly, a few neurons with strong α-syn staining in the cell body were detected in the brain sections of 12-month old *A53T* mice (Figures 4B, 4F). The occurrence of this abnormal somatic accumulation of α-syn was more prominent in the brain sections of 20-month old *A53T* mice (Figures 4C, 4G; Table 3), which was closely correlated with the progression of neurodegeneration in *A53T* mice, suggesting that the somatic accumulation of α-syn may trigger the pathogenic cascades leading to the cell death. We then investigated whether over-expression of *LRRK2* affects the subcellular distribution of α-syn. No obvious α-syn staining was found in the cell body of striatal neurons in 1 month-old *A53T* mice (Figure 4I). However, co-expression of *LRRK2* G2019S mutation greatly promoted the accumulation of α-syn in the soma of *A53T/G2019S* neurons in 1-month old mice (Figures 4J–L; Table 3). Similarly, increasing numbers of neurons with somatic accumulation of α-syn were detected in brain sections of 1-month old *A53T/LRRK2WT-L, A53T/LRRK2WT* and *A53T/KD* transgenic mice in a *LRRK2* dose-dependent manner (Figure 4M–4P; Table 3). To investigate whether over-expression of *LRRK2* G2019S mutation also promotes the accumulation of WT α-syn in the cell bodies, we examined the α-syn staining in brain sections from 20-month old *G2019S* mice and 1-month old human α-syn WT and G2019S double transgenic mice (α-*synWT/G2019S*). No apparent α-syn staining was detected in the soma of neurons in *G2019S* and α-*synWT* single transgenic mice (Supplemental Figure S6). By contrast, somatic staining of α-syn was apparent in neurons of 1-month old α-*synWT/G2019S* double transgenic mice (Supplemental Figure S6). These results suggest that the *LRRK2*-induced somatic accumulation of α-syn is independent of the presence of PD-related α-syn mutation but relies on the expression level of α-syn.

The staining of LRRK2 seemed to partially overlap with that of α-syn in the soma (Figures 4L, 4P). However, co-immunoprecipitation experiments failed to pull down LRRK2 and α-syn together from brain homogenates of *A53T/G2019S* and *A53T/LRRK2WT* mice (unpublished data). In addition, a few neurons, which showed obvious α-syn staining in the soma, were lack of substantial expression of *LRRK2* transgene (asterisk, Figures 4L, 4P). These observations suggest that LRRK2 may not directly bind to α-syn and prevent its trafficking to the axon terminals.

LRRK2 promoted the formation of α-syn aggregates

To examine if increased somatic accumulation of α-syn correlates with the formation of α-syn aggregates, we compared the levels of α-syn protein in total and sequentially detergent-extracted fractions of brain homogenates from 1 and 12-month old *A53T* transgenic mice. The formation of α-syn aggregates was detected as α-syn-positive high molecular weight (HMW) bands in the total brain homogenates of *A53T* mice (Figure 5). Interestingly, the intensity of HMW bands was significantly enhanced in the samples of 12-month old *A53T* mice as

compared to 1-month old animals (Figure 5A). We then examined the presence of α-syn aggregates in the Triton X100-insoluble (TX-insol) fractions of brain extracts. While the level of Triton X100-soluble (TX-sol) α-syn was comparable between these two age groups, a significant increase of TX-insol HMW α-syn was found in the samples of 12-month old *A53T* mice (Figure 5B). These data indicate the accumulation of α-syn in the soma may favor the formation of α-syn aggregates or *vise versa*.

Since over-expression of *LRRK2* promoted the somatic accumulation of α-syn, we reasoned that *LRRK2* may also promote the aggregation of α-syn. We therefore compared the level of HMW α-syn in the total brain lysates of 1-month old *A53T* and age-matched *A53T/G2019S* transgenic mice. A modest increase of HMW α-syn was detected in the *A53T/G2019S* samples (Figure 5C). Similarly, significantly more α-syn was detected in the TX-insoluble fraction of brain homogenates from *A53T/G2019S* transgenic mice (Figures 5D–E, $p = 0.033$). Together, these observations indicate that G2019S *LRRK2* promotes the formation of α-syn aggregates in neurons.

To test if α-syn is a potential substrate of LRRK2's kinase activity, we examined the phosphorylation of α-syn in total brain homogenates derived from one-month old *A53T* and *A53T/G2019S* transgenic mice (Figures 5D–E). Unexpectedly, we observed a reduction of α-syn phosphorylation at serine 129 in the brain lysate of double transgenic mice compared with that of *A53T* single transgenic animals ($p = 0.001$). This observation indicates that α-syn is unlikely to be a physiological substrate of LRRK2's kinase activity *in vivo*. Secreted α-syn is also implied in the pathogenesis of PD (Lee et al., 2005). To investigate if LRRK2 affects the secretion of α-syn, we measured the level of α-syn in cerebral spinal fluid (CSF) by ELISA. We found no significant alteration of secreted α-syn in *A53T/G2019S* double transgenic mice as compared to *A53T* single transgenic mice (data not shown).

Co-expression of *LRRK2* and *A53T* led to severe fragmentation of Golgi complex in neurons

Recent studies indicate that over-expression of either WT or PD-related mutant α-syn disrupts ER-Golgi traffic and causes Golgi fragmentation (Cooper et al., 2006;Gosavi et al., 2002). Interestingly, LRRK2 is associated with Golgi apparatus (Biskup et al., 2006). We therefore decided to examine the ER and Golgi structures in neurons of *A53T* and *LRRK2* single and double transgenic mice. There was no apparent change of ER structure in these neurons as revealed by calnexin staining (data not shown). However, the structure of Golgi complex was drastically altered in neurons of 1-month old *A53T/LRRK2* double transgenic mice (Figure 6). The morphology of Golgi apparatus was examined by GM130 and GLG1 staining, which recognizes cis and medial/trans-Golgi apparatus respectively. GM130 staining revealed tubular structures largely stacked at one side of neurons in 1-month old *nTg* and *A53T* mice (arrows, Figures 6A, 6D), which was classified as "Normal" Golgi. The GM130-positive tubules, however, appeared thinner and fragmented in neurons of *LRRK2WT* and *G2019S* mice (Figures 6B–C). When A53T was co-expressed with either WT or G2019S *LRRK2*, severe fragmentation of cis-Golgi was found (asterisk, Figures 6E–F), which was designed as "Fragmented" Golgi thereafter; and the partially fragmented Golgi was referred as "Intermediate" Golgi. Interestingly, the degree of Golgi apparatus fragmentation was correlated with the somatic accumulation of α-syn in these neurons (asterisks, Figures 6H–I). By contrast, neurons that lacked substantial α-syn staining in the soma displayed fairly normal appearance of cis-Golgi network (arrows, Figures 6E–F, Figures 6H–I). The prevalence of cis-Golgi fragmentation was quantified, which showed a significant decrease of "Normal" Golgi in *LRRK2* single and *A53T/LRRK2* double transgenic neurons as compared to *nTg* controls (Figure 6P). Meanwhile, the ratio of "Fragmented" Golgi was significantly elevated in neurons of *A53T/LRRK2* double transgenic mice (Figure 6P). We also examined the integrity of cis-Golgi network in striatal neurons of 6-month old animals and observed a similar fragmentation

of GM-130-posotive Golgi apparatus in *LRRK2WT, G2019S,* and *A53T/LRRK2* double transgenic neurons (Supplemental Figure S7). Interestingly, a significant increase of Golgi fragmentation was observed in neurons of 6-month old A53T mice (Supplemental Figure S7).

We then checked the structural integrity of medial/trans- Golgi in neurons of *A53T* and *LRRK2* mutant mice. In control *nTg* mice, GLG1 staining revealed the "Normal" perinuclear and polarized localization of Golgi stacks in neurons (arrows, Figure 6J). However, GLG1-staining was significantly altered in *LRRK2WT, G2019,* and *A53T* neurons and was shown as tubular structures scattered around the nucleus (arrowheads, Figures 6K–M). In *A53T/LRRK2WT* and *A53T/G2019S* neurons, with a few exceptions (arrowheads, Figures 6N–O,), the GLG1-staining was dispersed as small puncta or became indistinguishable from the background staining (asterisks, Figures 6N–O). We classified these dispersed structures as "Fragmented" Golgi. The ratio of "Fragmented" trans-Golgi was calculated, which was significantly increased in *A53T* and *LRRK2* single and double transgenic neurons as compared to *nTg* controls (Figure 6Q). Increased fragmentation of Golgi apparatus was also observed in neurons of *KD* and *A53T/KD* mice (Figures 6P–Q). Together these observations demonstrate that over-expression of *LRRK2* and α*-syn* severely disrupted the structure of Golgi apparatus, which may impair the ER/Golgi trafficking and contribute to the somatic accumulation of α-syn.

Over-expression of *LRRK2* perturbed the dynamics of microtubule assembly in *LRRK2* and *A53T/LRRK2* transgenic mice

Microtubule and microtubule-based intracellular transport play a critical role in maintaining the structure and function of Golgi apparatus (Thyberg and Moskalewski, 1999). LRRK2 has been shown to physically interact with both α and β tubulin through its GTPase domain (Gandhi et al., 2008;Gillardon, 2009). Consistently, we found that both WT and G2019S LRRK2 co-stained with βIII tubulin in the soma and proximal processes of striatal neurons in 1 and 6-month old *LRRK2* single and *A53T/LRRK2* double transgenic mice (Figure 7; Supplemental Figure S8). A significant overlap of somatic α-syn and βIII tubulin staining was also observed in neurons of 6-month old *A53T* single transgenic mice (Supplemental Figure S8) as well as in neurons of 1 and 6-month old *A53T/LRRK2WT* and *A53T/G2019S* double transgenic mice (Figures 7Dc–Dd, Supplemental Figure S8). These observations were consistent with the previous report that prefibrillar cytoplasmic α-syn interacts with tubulin in cell cultures (Lee et al., 2006).

To reveal the functional impact of *LRRK2* over-expression on the dynamics of microtubule organization, we compared the level of β-tubulin in both the Reassembly High-salt Buffer (RAB)-soluble and insoluble fractions of mouse brain homogenates from 1-month old *A53T, LRRK2WT* and *G2019S* single, and *A53T/LRRK2* double transgenic animals as well as *nTg* controls (Figures 7G–I). RAB buffer is generally used to extract intracellular free tubulin and cold-labile microtubules from brain homogenates (Weingarten et al., 1975). A dramatic reduction of β-tubulin was observed in the RAB-soluble (RAB-S) fraction of brain homogenates in *LRRK2WT, G2019S, and A53T/LRRK2* transgenic mice as compared to *nTg* controls and *A53T* single transgenic mice (Figures 7G–H). Concomitantly, more β-tubulin was found in the RAB-insoluble pellets (RAB-P) of *LRRK2* over-expressing mouse brains as compared to *nTg* and *A53T* samples (Figures 7G, 7I). The total level of β-tubulin, meanwhile, was comparable among all different genotypes (Supplemental Figure S9). The distribution of α-tubulin followed the same pattern as β-tubulin in the RAB-extracted brain homogenates from LRRK2 transgenic mice (data not shown). Taken together, these findings are consistent with previous *in vitro* assays that over-expression of *LRRK2* may enhance the polymerization of tubulin in cells (Gillardon, 2009), suggesting that the impairment of microtubule assembly may

affect the organization of microtubule network in the cell, resulting in the fragmentation of Golgi apparatus.

Over-expression of *LRRK2* and *A53T* impaired ubiquitin-proteasome system in both *A53T* and *LRRK2* transgenic mice

α-syn aggregates have been shown previously to impair the proteasomal and lysosomal activities that leads to accumulation of ubiquinated proteins in cells (Cuervo et al., 2004;Tanaka et al., 2001). Consistently, an elevation of ubiquitin (Ubi) staining was observed in the soma and nucleus of cortical neurons from 6-month old *A53T* mice (arrows, Figure 8Aa) but not from *nTg* controls (Figure 8Ae). The Ubi staining was partially overlapped with α-syn (Figure 8Ca). The pattern of Ubi staining was altered in 20-month old *A53T* mice, which displayed a punctuated staining pattern at neuron processes with no apparent co-localization with α-syn staining (arrowheads, Figures 8Ab, 8Cb). In the presence of excess WT *LRRK2*, a slightly more α-syn and Ubi-positive clusters were observed in brain sections of 6-month old *A53T/LRRK2WT* mice (arrowheads, Figure 8Bc). Interestingly, the presence of *G2019S* seemed to alter the Ubi-staining pattern to a more perinuclear location in neurons of *A53T/G2019S* mice (arrow, Figure 8Ad).

We then examined the Ubi staining in *LRRK2* transgenic mice. The level of Ubi staining was increased in cortical neurons of 6-month old *LRRK2WT* and *G2019S* mice (Figure 8D). Interestingly, the occurrence of Ubi-positive clusters was more prominent in *G2019S* neurons (arrowheads, Figure 8D). These Ubi-positive clusters appeared co-stained with LRRK2 in *G2019S* neurons (arrowheads, Figure 8F). This phenomenon became more apparent in neurons of 20-month old *G2019S* mice in which LRRK2 and Ubi staining were tightly co-localized as clusters (arrowheads, Figure 8Fe). Moreover, the presence of A53T α-*syn* accelerated the clustering of LRRK2 staining in neurons of *A53T/G2019S* mice (arrowheads, Figures 8Ed, 8Fd) as compared to age-matched *G2019S* mice (Figures 8Dc, 8Fc). In contrast, no obvious LRRK2-positive clusters were found in neurons of 6-month old *LRRK2WT* and *A53T/LRRK2WT* mice (Figures 8Da–b, 8Fa–b). Taken together, these observations indicate that G2019S *LRRK2* may further inhibit UPS activities, resulting in more frequent formation of LRRK2 and Ubi-positive aggregates in neurons of aged *G2019S* mice (Figures 8De, 8Ee). Our studies also indicate that the presence of A53T α-*syn* and G2019S *LRRK2* may cause synergistic impairment of ubiquitin-proteasome system (UPS) activities, which further accelerates the formation of LRRK2/Ubi-positive aggregates in neurons of *A53T/G2019S* double transgenic mice (Figures 8Dd, 8Ed).

In parallel with immunohistological studies, we also checked the levels of ubiquitinated proteins in brain homogenates of *A53T, LRRK2WT, G2019S, A53T/LRRK2WT*, and *A53T/G2019S* mice by Western blots (Figure 8G). A significant elevation of ubiquitination was observed in the brain homogenate of 3-month old *A53T* and *A53T/LRRK2WT* mice as compared to age-matched *nTg, LRRK2WT*, and *G2019S* mice (Figure 8H). The level of ubiquitination, however, was only moderately increased in the brain samples of 18-month old *G2019S* mice compared to age-matched *nTg* controls (Figures 8G–H).

LRRK2 exacerbated mitochondrial structural and functional abnormalities in neurons of *A53T* transgenic mice

Mitochondrial dysfunction has been shown in cell and mouse models over-expressing PD-related mutant α-syn (Hsu et al., 2000;Martin et al., 2006). We examined the morphology of mitochondria in striatal neurons of 1-month old mice by EM and found distinctive structural changes in some of the mitochondria in *A53T* and *A53T/G2019S* neurons. Compared to *nTg* and *G2019S* samples, the matrix of these abnormal mitochondria was denser (large arrows in Figures 9C–D, 9G–H), and the cristae became widened (small arrows in Figure 9G). The

frequency of such abnormal mitochondria was 52/1000 μm^2 in striatal area of *A53T* mice and ~3.5 times higher in *A53T/G2019S* double transgenic mice (184/1000 μm^2); whereas virtually none was found in age-matched *nTg* or *G2019S* transgenic mice (Figures 9A–D). The abnormal mitochondria were preferentially distributed in dendrites/soma, with only a few in axon terminals (unpublished data). The mitochondrial structural abnormalities were also confirmed by immunostaining with an antibody against cytochrome c oxidase subunit I, a mitochondrial inner membrane protein (supplemental Figure S10).

To address whether the morphological abnormalities affect the function of mitochondria in striatal neurons of 1-month old *A53T* and *A53T/G2019S* transgenic mice, we infused the animal with MitoSox Red, a fluorescent dye for detecting the surplus of mitochondrial superoxide released to the matrix (Robinson et al., 2006). MitoSox Red signal was easily detected in the brain of *A53T/G2019S* transgenic mice and was more prominent in the dorsal lateral striatum (Figures 9L–M), where most neurodegeneration was found. In contrast, only a few MitoSox Red-positive neurons were found in the stratum of *A53T* mice (arrowhead, Figure 9K) and no positive staining was detected in *nTg* or *G2019S* transgenic mice (Figures 9I–J). These results suggest that co-expression of α-*syn* and *LRRK2* cause synergistic toxicity to mitochondria.

Inhibition of LRRK2 expression ameliorated α-syn-mediated neuropathology

Since over-expression of *LRRK2* accelerated the progression of α-syn-induced neuropathological abnormalities, we decided to investigate whether inhibition of *LRRK2* expression was able to alleviate the pathogenesis of mutant α-syn. To inhibit *LRRK2* expression, we generated *LRRK2* knockout (*LRRK2*$^{-/-}$) mice (Supplemental Figure S11). *LRRK2*$^{-/-}$ mice were viable, fertile, and displayed no obvious motor behavioral phenotypes (Supplemental Figure S12). No apparent elevation of reactive astrocytosis, neurodegeneration, or somatic accumulation of α-syn was found in brains of 20-month old *LRRK2*$^{-/-}$ mice (Supplemental Figure S12; Table 1–Table 3). Furthermore, the levels of α-syn in Triton-X100 insoluble fraction appeared comparable between *LRRK2*$^{+/+}$ and *LRRK2*$^{-/-}$ mice, indicating no apparent α-syn aggregates were formed in *LRRK2*$^{-/-}$ mouse brains (data not shown). Compared to littermate controls, only a moderate increase of activated microglia (Supplemental Figure S12; Table 2) was observed in the brain of 20-month old *LRRK2*$^{-/-}$ mice.

To generate *A53T* mice in the *LRRK2* knockout background (*A53T/LRRK2*$^{-/-}$), we intercrossed *tetO-A53T/LRRK2*$^{+/-}$ and *CaMKII-tTA/LRRK2*$^{+/-}$ mice to get *A53T/LRRK2*$^{-/-}$and littermate control mice. The neuropathology of *A53T/LRRK2*$^{-/-}$ mice and littermate controls was examined at 6 and 12 months of age (Supplemental Figure S13; Figure 10). Similar to *A53T/LRRK2*$^{+/+}$ mice, 12-month old *A53T/LRRK2*$^{+/-}$ mice also displayed significant neurodegeneration, astrocytosis, microgliosis, somatic accumulation of α-syn and severe fragmentation of Golgi apparatus in the striatum (Figure 10). In contrast, no apparent neurodegeneration was found in the striatum of age-matched littermate *A53T/LRRK2*$^{-/-}$ mice (Figure 10Ab; Table 1). The number of residual neurons in the striatum of 12-month old *A53T/LRRK2*$^{-/-}$ is also significantly more as compared to age-matched *A53T/LRRK2*$^{+/-}$ and *A53T/LRRK2*$^{+/+}$ mice (Figure 10F). Moreover, no significant elevation of astrocytosis, microgliosis, or somatic accumulation of α-syn was detected in the striatum of 12-month old *A53T/LRRK2*$^{-/-}$ mice (Figure 10; Table 2 and Table 3). GLG1 staining revealed normal morphology and distribution of Golgi apparatus in neurons of *A53T/LRRK2*$^{-/-}$ mice (Figures 10Eb, 10J). Similar rescuing effects were also observed in the brain of 12-month old *A53T/LRRK2*$^{+/+}$ mice treated with doxycycline (*A53T/DOX*) (Figure 10). Stereological analyses further revealed significant reduction of neurodegeneration in *A53T/DOX* mice as compared to age-matched *A53T/LRRK2*$^{+/+}$ mice (Figure 10F). In addition to immunohistological analyses, Western blots revealed a significant decrease of HMW α-syn in the total brain homogenates of *A53T/LRRK2*$^{-/-}$ mice as compared to age-matched *A53T/LRRK2*$^{+/-}$ mice (Figures 10G, 10I). By

contrast, only a moderate decrease of HMW-Ubi was observed in *A53T/LRRK2*$^{-/-}$ samples (Figure 10G), which did not reach statistical significance by the densitometry analysis. Together these findings demonstrated that inhibition of *LRRK2* expression successfully ameliorated α-syn-mediated neuropathological abnormalities in *A53T* transgenic mice.

Discussion

Mutations in α-*syn* or *LRRK2* lead to typical PD-like neuropathological features such as the formation of α-syn-containing cytoplasmic inclusion, Lewy bodies (LB) (Hardy et al., 2006). LRRK2-immunoreactivity is also associated with LB (Higashi et al., 2007;Zhu et al., 2006). The expression of α-*syn* and *LRRK2* appears co-regulated in the mouse striatum (Westerlund et al., 2008). These early studies indicate a potential pathophysiological interplay between α-*syn* and *LRRK2*. To systematically investigate whether α-*syn* and *LRRK2* act synergistically in the pathogenesis of PD, we generated and characterized a series of compound transgenic mice over-expressing PD-related A53T α-*syn* mutant with various forms of *LRRK2*. Here we show that *LRRK2* regulated the progression of neuropathological abnormalities induced by A53T α-*syn*. Over-expression of either wild-type or PD-associated G2019S *LRRK2* greatly accelerated the progression of A53T α-*syn*-mediated neurodegeneration. At the cellular level, over-expression of *LRRK2* impaired microtubule dynamics and caused Golgi fragmentation, which we suspect might exacerbate A53T α-*syn*-induced cytotoxicity via promoting the abnormal somatic accumulation of α-syn. By contrast, genetic ablation of *LRRK2* maintained the normal organization of Golgi complex, reduced the aggregation and somatic accumulation of A53T α-syn, and thereby significantly delayed the progression of A53T α-syn-induced neuropathology.

PD is clinically characterized as dyskinesia, resting tremor, rigidity, and abnormal posture. The lack of obvious PD-like behavioral phenotypes in our *G2019S* and *A53T* mutant mice might be attributed to the scarce expression of exogenous *LRRK2* and α-*syn* transgenes in midbrain dopaminergic (DA) neurons under the *CaMKII* promoter. Therefore, our present *A53T* and *G2019S* transgenic mice are not ideal for studying the dysfunction of DA neurons. Nevertheless, they may serve as useful tools to investigate the pathogenic mechanisms of PD-related mutant *LRRK2* and α-*syn in vivo*. Currently, we are in the process of generating new lines of mice, which over-express G2019S *LRRK2* or A53T α-*syn* in midbrain DA neurons. It would be interesting to determine whether G2019S *LRRK2* and A53T α-*syn* have the same synergistic toxic effect when co-expressed in DA neurons.

PD is pathologically characterized by the presence of α-syn-containing inclusion bodies in the perinuclear area (Spillantini et al., 1997). However, in normal neurons, α-syn is typically enriched at axon terminals where it is associated with synaptic vesicles (Maroteaux and Scheller, 1991;Tao-Cheng, 2006). Like other synaptic vesicle proteins, the secretion of α-syn is mediated by the ER-Golgi network and transported to the axonal terminals by microtubule-based motor proteins (Roy et al., 2008). Therefore, the formation of somatic inclusion of α-syn may result from the dysfunction of ER/Golgi trafficking and microtubule-based axonal transport (Cooper et al., 2006;Gosavi et al., 2002). As an extension of these previous *in vitro* observations, we found a significant increase of fragmented Golgi apparatus in neurons of 6 and 12-month old A53T α-*syn* transgenic mice, which is correlated with an increased prevalence of neurons with somatic accumulation of α-syn. Interestingly, over-expression of either WT or G2019S *LRRK2* greatly promoted the abnormal somatic accumulation of both the WT and A53T α-syn in neurons. LRRK2 has been shown to associate with Golgi complex (Biskup et al., 2006). While we did not observe any substantial co-staining of LRRK2 and Golgi in *LRRK2* transgenic neurons (data not shown), we found that over-expression of LRRK2 caused significant fragmentation of Golgi complex. Moreover, co-expression of *LRRK2* and α-*syn* led to more severe and synergistic fragmentation of Golgi apparatus, which was tightly

correlated with the augmentation of α-syn accumulation in the soma. By contrast, inhibition of *LRRK2* expression prevented the disintegration of Golgi complex in *A53T* neurons and suppressed the accumulation of α-syn in cell bodies. Together, our present study reveals a novel function of LRRK2 in maintaining the normal organization of Golgi apparatus and further demonstrates that the dysfunction of ER-Golgi-mediated protein/vesicle trafficking may contribute significantly to α-syn-induced pathogenesis in PD.

In mammalian cells, Golgi apparatus is composed of multiple layers of cisternal stacks juxtaposed with microtubule organization center in the vicinity of the nucleus and microtubules play an important role in maintaining the organization of Golgi complex (Thyberg and Moskalewski, 1999). In line with this notion, Lee and colleagues recently showed that α-syn co-aggregates with microtubules and impairs microtubule-dependent vesicle trafficking, which is proposed as a potential molecular mechanism underlying α-syn-induced Golgi fragmentation in cell cultures (Lee et al., 2006). Interestingly, LRRK2 has been shown to physically interact with both α and β-tubulin through its GTPase domain (Gandhi et al., 2008;Gillardon, 2009). Various microtubule-associated proteins, including tau, regulate the stability and dynamics of microtubule network (Valiron et al., 2001). In line with this notion, a recent report suggests that G2019S LRRK2 preferentially phosphorylates β-tubulin purified from brain tissues and enhances the assembly of microtubules in the presence of other microtubule-associated proteins (Gillardon, 2009). In contrast, the level of free tubulin is significantly increased in the brain extract of *LRRK2*$^{-/-}$ mice (Gillardon, 2009). In agreement with these early observations, we found that the level of RAB-insoluble tubulin was significantly elevated in the brain homogenate of *LRRK2* transgenic mice as compared with *nTg* controls and *A53T* single transgenic mice; whereas, the level of RAB-soluble tubulin was dramatically decreased in the brain homogenate of *LRRK2* single and *A53T/LRRK2* double transgenic mice. While the total levels of α and β-tubulin in the brain homogenates were not affected in *LRRK2* transgenic mice, the altered ratio of RAB-soluble *vs*. RAB-insoluble tubulin in *LRRK2* over-expressing neurons may reflect a depletion of the free pool subunits and thereby a significant enhancement of tubulin polymerization. Previous studies demonstrated that the treatment of taxol, a microtubule stabilizer, leads to redistribution of microtubules in the cell and fragmentation of Golgi apparatus into areas of cells rich in microtubules (Wehland et al., 1983). Therefore, we suspect a similar sequence of events occurred in neurons over-expressing *LRRK2* in which LRRK2 increases of the ability of tubulin to polymerize, disrupts the normal microtubule organization, and as the consequence, alters the normal distribution of Golgi complex. The fragmentation of Golgi apparatus *per se* may not cause overt cytotoxicity, but it could impair the efficiency of coordinated vesicle trafficking in mammalian cells (Thyberg and Moskalewski, 1999), which may explain why over-expression of *LRRK2* alone did not cause any neurodegeneration albeit apparent Golgi fragmentation; while together with A53T α-syn, LRRK2 dramatically accelerated the abnormal somatic accumulation of α-syn and associated cell loss. Together with previous *in vitro* studies (Gandhi et al., 2008;Gillardon, 2009), our findings indicate that LRRK2 is a stabilizer of microtubule assembly in cells and over-expression of *LRRK2* promotes the additional polymerization of tubulin in neurons, which we suspect might lead to the fragmentation of Golgi apparatus and exacerbate α-syn-induced ER/Golgi trafficking defects and other cytotoxicities.

The increased accumulation of α-syn in the soma may favor the formation of α-syn aggregates, a key factor underlying its toxicity to neurons (Conway et al., 1998; Narhi et al., 1999). Concurrent with somatic accumulation of α-syn, more HMW and detergent-insoluble α-syn was detected in the brain homogenate of aged *A53T* and *A53T/G2019S* mice. Previous studies indicate that α-syn aggregates cause proteasome impairment (Tanaka et al., 2001), which may lead to the accumulation of ubiquitinated proteins in neurons. Consistently, the levels of ubiquitinated proteins were up-regulated in *A53T* and aged *G2019S* mice. Moreover, G2019S LRRK2 mutant protein was sequestered as ubiquitin-positive clusters in neurons of aged

animals. We have shown earlier that the degradation of LRRK2 is primarily through the proteasomal pathway (Wang et al., 2008). The accumulating of G2019S mutant and ubiquitin-positive protein aggregates in aged mice indicate that over-expression of LRRK2, especially the G2019S mutant, may impair the UPS activities in neurons. Moreover, the presence of A53T α-syn seemed to further damage the UPS activity and accelerate the sequestration of *LRRK2* G2019S aggregates. Although the UPS activities were apparently impaired in neurons of *A53T* mice, the dysfunction of UPS activities might not play a main role in A53T-mediated neuropathogenesis in our mouse model, since the inhibition of *LRRK2* expression, which dramatically delayed the progression of neurodegeneration in *A53T* mice, only moderately reduced the accumulation of HMW ubiquitinated proteins. These observations further support the notion that the dysfunction of Golgi and microtubule-based molecule/vesicle trafficking is likely a main pathogenic route of α-syn and LRRK2-mediated neurodegeneration.

Extensive efforts have been devoted to identify the potential physiological substrates of LRRK2's kinase activities (Imai et al., 2008;Jaleel et al., 2007), although no formal link has been established between the LRRK2's kinase activities and the pathogenesis of PD. To further address whether the putative protein kinase domain of LRRK2 is critical in regulating α-*syn*-mediated neuropathology, we generated *LRRK2* kinase-deletion (KD) inducible transgenic mice and crossbred these mice with *A53T* transgenic mice. Over-expression of *LRRK2* KD mutant also caused Golgi fragmentation and the impairment of microtubule dynamics. When co-expressed with A53T α-*syn*, *LRRK2* KD mutant promoted the somatic accumulation of α-*syn* A53T mutant and accelerated A53T-mediated neuropathology to a similar extent as *LRRK2* WT protein. These data suggest that the kinase domain of LRRK2 is likely not critical in accelerating *A53T*–induced neuropathological abnormalities. Instead, the GTPase domain of LRRK2 may play a more important role in LRRK2-induced damage to microtubules and Golgi apparatus through its direct association with microtubules. It will be interesting to evaluate the role of *LRRK2* GTPase domain in regulating the stability of microtubule network and ER/Golgi trafficking in neurons and its contribution to A53T α-*syn*-mediated neurodegeneration.

In summary, we have revealed a novel function of LRRK2 in regulating the intracellular trafficking and accumulation of α-syn in neurons. Our data suggest that excessive amount of LRRK2 or its mutants may impair the structure and function of Golgi complex and microtubule-based transport, resulting in abnormal somatic accumulation of α-syn, which may contribute to the accelerated progression of neuropathology induced by α-*syn* A53T mutant. Generally, pathogenic proteins of human origin need to be overly expressed in order to reproduce the desired behavioral and pathological phenotypes in transgenic mouse models, which also raise concerns on disease-unrelated cytotoxicity. While an 8 to 16-fold increase of LRRK2 protein expression in *LRRK2WT* and *G2019S* mice greatly exacerbated α-*syn* A53T-mediated cytotoxicity, a moderate increase of LRRK2 expression in both *LRRK2WT-L* and *KD* mice also enabled to promote α-*syn* A53T-induced neurodegeneration. These findings suggest that the synergistic cytotoxicity induced by co-expression of α-*syn* A53T and *LRRK2* could not be simply attributed to the excess expression of *LRRK2*. Instead, our study indicates that *LRRK2* may process an intrinsic function in regulating the progression of α-*syn* A53T-mediated neuropathological abnormalities. In support of this notion, genetic inhibition of *LRRK2* expression in α-*syn* A53T transgenic mice significantly reduced the fragmentation of Golgi complex and somatic accumulation of α-syn in neurons, and effectively delayed the progression of α-*syn* A53T-mediated neuropathological abnormalities. These results also suggest that inhibition of *LRRK2* expression may provide an applicable therapeutic strategy to ameliorate α-syn-induced neurodegeneration in PD or other related neurodegenerative diseases.

Experimental Procedures

Generation of *LRRK2* and α-*synuclein* Inducible Transgenic Mice and *LRRK2*$^{-/-}$ mice

The generation of human WT and KD *LRRK2*, as well as WT and A53T α-*syn* inducible transgenic mice was followed the same protocol as described previously for the development of G2019S LRRK2 transgenic mice (Wang et al., 2008). The *LRRK2*$^{-/-}$ mice were generated through deletion the second coding exon of *LRRK2* (Parisiadou et al., 2009, in press). All mouse work follows the guidelines approved by the Institutional Animal Care and Use Committees of the National Institute of Child Health and Human Development.

Immunohistochemistry and Light Microscopy

The detailed information about immunohistochemical procedures was provided in Supplemental Materials. Three or more animals per genotype and age group were used for each study. Fluorescence images were captured using a laser scanning confocal microscope (LSM 510; Zeiss, Thornwood, NJ). The paired images in all the figures were collected at the same gain and offset settings. When post collection processing was done, it was applied uniformly to all paired images. The images of α-syn staining were presented as a single optic layer after acquired in *z*-series stack scans at 0.8 μm intervals.

Stereology

According to stereotaxic coordinates (3rd edition, Keith B.J. Franklin and George Paxinos), series of coronal sections across the dorsal striatum were processed for TH and GFAP as well as TH and NeuN co-staining. Three or more animals per genotype and age group were used for each study. The numbers of GFAP and NeuN-positive cells was assessed using Stereo Investigator 8 (MicroBrightField Inc, Williston, VT). The sampling scheme was designed to have coefficient of error (CE) less than 10% in order to get reliable results. All stereological analyses were performed under the 100 × objective of a Zeiss Axio microscope (Imager A1).

Extraction of tubulin from mouse brains

As described previously (Ishihara et al., 1999), freshly dissected mouse brains were homogenized in 2ml/g of RAB Hi-Salt buffer [0.1M morpholineethanesulfonic acid (MES), 1mM EGTA, 0.75M NaCl, 0.02M NaF, 0.5mM $MgSO_4$, 1mM PMSF, 100mM EDTA)] and protease inhibitors cocktail and centrifuged at 50, 000 × g for 1 hour. The pellets (RAB-P) were saved and the RAB-extractable supernatants were boiled for 5 min and then chilled on ice for another 5 min. In turn, they were centrifuged at 10, 000 × g for 20 min at 4°C. Both the pellets and the supernatants (RAB-S) were saved. After protein concentration was determined using the BCA assay kit (Pierce), equal amount of proteins from RAB-P and RAB-S fractions was analyzed by Western Blot.

Statistical Analysis

Statistical analysis was performed using Graphpad Prism 5 (Graphpad Software Inc. La Jolla, CA) and StatView program (SAS Institute Inc.). Data are presented as means ± SEM. Statistical significances were determined by comparing means of different groups using t-test or ANOVA followed by Post Hoc Tukey HSD test.

Supplementary Material

Refer to Web version on PubMed Central for supplementary material.

Acknowledgments

This work was supported in part by the intramural research programs of National Institute on Aging, National Human Genome Research Institute (NHGRI), National Institute of Mental Health (NIMH), and National Institute of Neurological Disorders and Stroke (NINDS) at the National Institutes of Health and the Henry Jackson Foundation. We thank the NHGRI and NIMH transgenic mouse facilities for blastocystic and pronuclear injections; the NINDS DNA Sequence Facility for sequencing DNA constructs; Dr. David Borchelt for kindly providing the tetO expression vector; Drs. Darren Moore, Valina Dawson, Ted Dawson (the Johns Hopkins University School of Medicine) and Jean-Marc Taymans (Universiteit Leuven) for kindly providing LRRK2 antibodies; Drs. John Hardy and Andy Singleton for their helpful suggestions; and the NIH Fellows Editorial Board for editing this manuscript.

Reference List

1. Arlotta P, Molyneaux BJ, Jabaudon D, Yoshida Y, Macklis JD. Ctip2 controls the differentiation of medium spiny neurons and the establishment of the cellular architecture of the striatum. J.Neurosci 2008;28:622–632. [PubMed: 18199763]
2. Biskup S, Moore DJ, Celsi F, Higashi S, West AB, Andrabi SA, Kurkinen K, Yu SW, Savitt JM, Waldvogel HJ, Faull RL, Emson PC, Torp R, Ottersen OP, Dawson TM, Dawson VL. Localization of LRRK2 to membranous and vesicular structures in mammalian brain. Ann.Neurol 2006;60:557–569. [PubMed: 17120249]
3. Conway KA, Harper JD, Lansbury PT. Accelerated in vitro fibril formation by a mutant alpha-synuclein linked to early-onset Parkinson disease. Nat.Med 1998;4:1318–1320. [PubMed: 9809558]
4. Cooper AA, Gitler AD, Cashikar A, Haynes CM, Hill KJ, Bhullar B, Liu K, Xu K, Strathearn KE, Liu F, Cao S, Caldwell KA, Caldwell GA, Marsischky G, Kolodner RD, Labaer J, Rochet JC, Bonini NM, Lindquist S. Alpha-synuclein blocks ER-Golgi traffic and Rab1 rescues neuron loss in Parkinson's models. Science 2006;313:324–328. [PubMed: 16794039]
5. Cuervo AM, Stefanis L, Fredenburg R, Lansbury PT, Sulzer D. Impaired degradation of mutant alpha-synuclein by chaperone-mediated autophagy. Science 2004;305:1292–1295. [PubMed: 15333840]
6. Galter D, Westerlund M, Carmine A, Lindqvist E, Sydow O, Olson L. LRRK2 expression linked to dopamine-innervated areas. Ann.Neurol 2006;59:714–719. [PubMed: 16532471]
7. Gandhi PN, Wang X, Zhu X, Chen SG, Wilson-Delfosse AL. The Roc domain of leucine-rich repeat kinase 2 is sufficient for interaction with microtubules. J.Neurosci.Res. 2008
8. Gilks WP, Abou-Sleiman PM, Gandhi S, Jain S, Singleton A, Lees AJ, Shaw K, Bhatia KP, Bonifati V, Quinn NP, Lynch J, Healy DG, Holton JL, Revesz T, Wood NW. A common LRRK2 mutation in idiopathic Parkinson's disease. Lancet 2005;365:415–416. [PubMed: 15680457]
9. Gillardon F. Leucine-rich repeat kinase 2 phosphorylates brain tubulin-beta isoforms and modulates microtubule stability - a point of convergence in Parkinsonian neurodegeneration? J.Neurochem. 2009
10. Gong S, Zheng C, Doughty ML, Losos K, Didkovsky N, Schambra UB, Nowak NJ, Joyner A, Leblanc G, Hatten ME, Heintz N. A gene expression atlas of the central nervous system based on bacterial artificial chromosomes. Nature 2003;425:917–925. [PubMed: 14586460]
11. Gosavi N, Lee HJ, Lee JS, Patel S, Lee SJ. Golgi fragmentation occurs in the cells with prefibrillar alpha-synuclein aggregates and precedes the formation of fibrillar inclusion. J.Biol.Chem 2002;277:48984–48992. [PubMed: 12351643]
12. Greggio E, Jain S, Kingsbury A, Bandopadhyay R, Lewis P, Kaganovich A, van der Brug MP, Beilina A, Blackinton J, Thomas KJ, Ahmad R, Miller DW, Kesavapany S, Singleton A, Lees A, Harvey RJ, Harvey K, Cookson MR. Kinase activity is required for the toxic effects of mutant LRRK2/dardarin. Neurobiol.Dis 2006;23:329–341. [PubMed: 16750377]
13. Hardy J, Cai H, Cookson MR, Gwinn-Hardy K, Singleton A. Genetics of Parkinson's disease and parkinsonism. Ann.Neurol 2006;60:389–398. [PubMed: 17068789]
14. Higashi S, Biskup S, West AB, Trinkaus D, Dawson VL, Faull RL, Waldvogel HJ, Arai H, Dawson TM, Moore DJ, Emson PC. Localization of Parkinson's disease-associated LRRK2 in normal and pathological human brain. Brain Res 2007;1155:208–219. [PubMed: 17512502]
15. Hsu LJ, Sagara Y, Arroyo A, Rockenstein E, Sisk A, Mallory M, Wong J, Takenouchi T, Hashimoto M, Masliah E. alpha-synuclein promotes mitochondrial deficit and oxidative stress. Am.J.Pathol 2000;157:401–410. [PubMed: 10934145]

16. Imai Y, Gehrke S, Wang HQ, Takahashi R, Hasegawa K, Oota E, Lu B. Phosphorylation of 4E-BP by LRRK2 affects the maintenance of dopaminergic neurons in Drosophila. EMBO J 2008;27:2432–2443. [PubMed: 18701920]

17. Ishihara T, Hong M, Zhang B, Nakagawa Y, Lee MK, Trojanowski JQ, Lee VM. Age-dependent emergence and progression of a tauopathy in transgenic mice overexpressing the shortest human tau isoform. Neuron 1999;24:751–762. [PubMed: 10595524]

18. Jaleel M, Nichols RJ, Deak M, Campbell DG, Gillardon F, Knebel A, Alessi DR. LRRK2 phosphorylates moesin at threonine-558: characterization of how Parkinson's disease mutants affect kinase activity. Biochem.J 2007;405:307–317. [PubMed: 17447891]

19. Jankowsky JL, Slunt HH, Gonzales V, Savonenko AV, Wen JC, Jenkins NA, Copeland NG, Younkin LH, Lester HA, Younkin SG, Borchelt DR. Persistent amyloidosis following suppression of Abeta production in a transgenic model of Alzheimer disease. PLoS.Med 2005;2:e355. [PubMed: 16279840]

20. Lee HJ, Khoshaghideh F, Lee S, Lee SJ. Impairment of microtubule-dependent trafficking by overexpression of alpha-synuclein. Eur.J.Neurosci 2006;24:3153–3162. [PubMed: 17156376]

21. Lee HJ, Patel S, Lee SJ. Intravesicular localization and exocytosis of alpha-synuclein and its aggregates. J.Neurosci 2005;25:6016–6024. [PubMed: 15976091]

22. Li X, Tan YC, Poulose S, Olanow CW, Huang XY, Yue Z. Leucine-rich repeat kinase 2 (LRRK2)/PARK8 possesses GTPase activity that is altered in familial Parkinson's disease R1441C/G mutants. J.Neurochem. 2007

23. Li Y, Liu W, Oo TF, Wang L, Tang Y, Jackson-Lewis V, Zhou C, Geghman K, Bogdanov M, Przedborski S, Beal MF, Burke RE, Li C. Mutant LRRK2(R1441G) BAC transgenic mice recapitulate cardinal features of Parkinson's disease. Nat.Neurosci 2009;12:826–828. [PubMed: 19503083]

24. Liu Z, Wang X, Yu Y, Li X, Wang T, Jiang H, Ren Q, Jiao Y, Sawa A, Moran T, Ross CA, Montell C, Smith WW. A Drosophila model for LRRK2-linked parkinsonism. Proc.Natl.Acad.Sci.U.S.A. 2008

25. Maroteaux L, Campanelli JT, Scheller RH. Synuclein: a neuron-specific protein localized to the nucleus and presynaptic nerve terminal. J.Neurosci 1988;8:2804–2815. [PubMed: 3411354]

26. Maroteaux L, Scheller RH. The rat brain synucleins; family of proteins transiently associated with neuronal membrane. Brain Res.Mol.Brain Res 1991;11:335–343. [PubMed: 1661825]

27. Martin LJ, Pan Y, Price AC, Sterling W, Copeland NG, Jenkins NA, Price DL, Lee MK. Parkinson's disease alpha-synuclein transgenic mice develop neuronal mitochondrial degeneration and cell death. J.Neurosci 2006;26:41–50. [PubMed: 16399671]

28. Mayford M, Bach ME, Huang YY, Wang L, Hawkins RD, Kandel ER. Control of memory formation through regulated expression of a CaMKII transgene. Science 1996;274:1678–1683. [PubMed: 8939850]

29. Narhi L, Wood SJ, Steavenson S, Jiang Y, Wu GM, Anafi D, Kaufman SA, Martin F, Sitney K, Denis P, Louis JC, Wypych J, Biere AL, Citron M. Both familial Parkinson's disease mutations accelerate alpha-synuclein aggregation. J.Biol.Chem 1999;274:9843–9846. [PubMed: 10092675]

30. Nichols WC, Pankratz N, Hernandez D, Paisan-Ruiz C, Jain S, Halter CA, Michaels VE, Reed T, Rudolph A, Shults CW, Singleton A, Foroud T. Genetic screening for a single common LRRK2 mutation in familial Parkinson's disease. Lancet 2005;365:410–412. [PubMed: 15680455]

31. Nussbaum RL, Polymeropoulos MH. Genetics of Parkinson's disease. Hum.Mol.Genet 1997;6:1687–1691. [PubMed: 9300660]

32. Paisan-Ruiz C, Jain S, Evans EW, Gilks WP, Simon J, van der BM, Lopez dM, Aparicio S, Gil AM, Khan N, Johnson J, Martinez JR, Nicholl D, Carrera IM, Pena AS, de Silva R, Lees A, Marti-Masso JF, Perez-Tur J, Wood NW, Singleton AB. Cloning of the gene containing mutations that cause PARK8-linked Parkinson's disease. Neuron 2004;44:595–600. [PubMed: 15541308]

33. Robinson KM, Janes MS, Pehar M, Monette JS, Ross MF, Hagen TM, Murphy MP, Beckman JS. Selective fluorescent imaging of superoxide in vivo using ethidium-based probes. Proc.Natl.Acad.Sci.U.S.A 2006;103:15038–15043. [PubMed: 17015830]

34. Roy S, Winton MJ, Black MM, Trojanowski JQ, Lee VM. Cytoskeletal requirements in axonal transport of slow component-b. J.Neurosci 2008;28:5248–5256. [PubMed: 18480281]

35. Savitt JM, Dawson VL, Dawson TM. Diagnosis and treatment of Parkinson disease: molecules to medicine. J.Clin.Invest 2006;116:1744–1754. [PubMed: 16823471]
36. Smith WW, Pei Z, Jiang H, Dawson VL, Dawson TM, Ross CA. Kinase activity of mutant LRRK2 mediates neuronal toxicity. Nat.Neurosci 2006;9:1231–1233. [PubMed: 16980962]
37. Spillantini MG, Schmidt ML, Lee VM, Trojanowski JQ, Jakes R, Goedert M. Alpha-synuclein in Lewy bodies. Nature 1997;388:839–840. [PubMed: 9278044]
38. Tanaka Y, Engelender S, Igarashi S, Rao RK, Wanner T, Tanzi RE, Sawa A, Dawson L, Dawson TM, Ross CA. Inducible expression of mutant alpha-synuclein decreases proteasome activity and increases sensitivity to mitochondria-dependent apoptosis. Hum.Mol.Genet 2001;10:919–926. [PubMed: 11309365]
39. Tao-Cheng JH. Activity-related redistribution of presynaptic proteins at the active zone. Neuroscience 2006;141:1217–1224. [PubMed: 16757121]
40. Thyberg J, Moskalewski S. Role of microtubules in the organization of the Golgi complex. Exp.Cell Res 1999;246:263–279. [PubMed: 9925741]
41. Tong Y, Pisani A, Martella G, Karouani M, Yamaguchi H, Pothos EN, Shen J. R1441C mutation in LRRK2 impairs dopaminergic neurotransmission in mice. Proc.Natl.Acad.Sci.U.S.A 2009;106:14622–14627. [PubMed: 19667187]
42. Trojanowski JQ, Goedert M, Iwatsubo T, Lee VM. Fatal attractions: abnormal protein aggregation and neuron death in Parkinson's disease and Lewy body dementia. Cell Death.Differ 1998;5:832–837. [PubMed: 10203692]
43. Valiron O, Caudron N, Job D. Microtubule dynamics. Cell Mol.Life Sci 2001;58:2069–2084. [PubMed: 11814057]
44. Wang L, Xie C, Greggio E, Parisiadou L, Shim H, Sun L, Chandran J, Lin X, Lai C, Yang WJ, Moore DJ, Dawson TM, Dawson VL, Chiosis G, Cookson MR, Cai H. The chaperone activity of heat shock protein 90 is critical for maintaining the stability of leucine-rich repeat kinase 2. J.Neurosci 2008;28:3384–3391. [PubMed: 18367605]
45. Wehland J, Henkart M, Klausner R, Sandoval IV. Role of microtubules in the distribution of the Golgi apparatus: effect of taxol and microinjected anti-alpha-tubulin antibodies. Proc.Natl.Acad.Sci.U.S.A 1983;80:4286–4290. [PubMed: 6136036]
46. Weingarten MD, Lockwood AH, Hwo SY, Kirschner MW. A protein factor essential for microtubule assembly. Proc.Natl.Acad.Sci.U.S.A 1975;72:1858–1862. [PubMed: 1057175]
47. West AB, Moore DJ, Biskup S, Bugayenko A, Smith WW, Ross CA, Dawson VL, Dawson TM. Parkinson's disease-associated mutations in leucine-rich repeat kinase 2 augment kinase activity. Proc.Natl.Acad.Sci.U.S.A 2005;102:16842–16847. [PubMed: 16269541]
48. Westerlund M, Ran C, Borgkvist A, Sterky FH, Lindqvist E, Lundstromer K, Pernold K, Brene S, Kallunki P, Fisone G, Olson L, Galter D. Lrrk2 and alpha-synuclein are co-regulated in rodent striatum. Mol.Cell Neurosci 2008;39:586–591. [PubMed: 18790059]
49. Zabetian CP, Samii A, Mosley AD, Roberts JW, Leis BC, Yearout D, Raskind WH, Griffith A. A clinic-based study of the LRRK2 gene in Parkinson disease yields new mutations. Neurology 2005;65:741–744. [PubMed: 16157909]
50. Zhu X, Siedlak SL, Smith MA, Perry G, Chen SG. LRRK2 protein is a component of Lewy bodies. Ann.Neurol 2006;60:617–618. [PubMed: 16847950]
51. Zimprich A, Biskup S, Leitner P, Lichtner P, Farrer M, Lincoln S, Kachergus J, Hulihan M, Uitti RJ, Calne DB, Stoessl AJ, Pfeiffer RF, Patenge N, Carbajal IC, Vieregge P, Asmus F, Muller-Myhsok B, Dickson DW, Meitinger T, Strom TM, Wszolek ZK, Gasser T. Mutations in LRRK2 cause autosomal-dominant parkinsonism with pleomorphic pathology. Neuron 2004;44:601–607. [PubMed: 15541309]

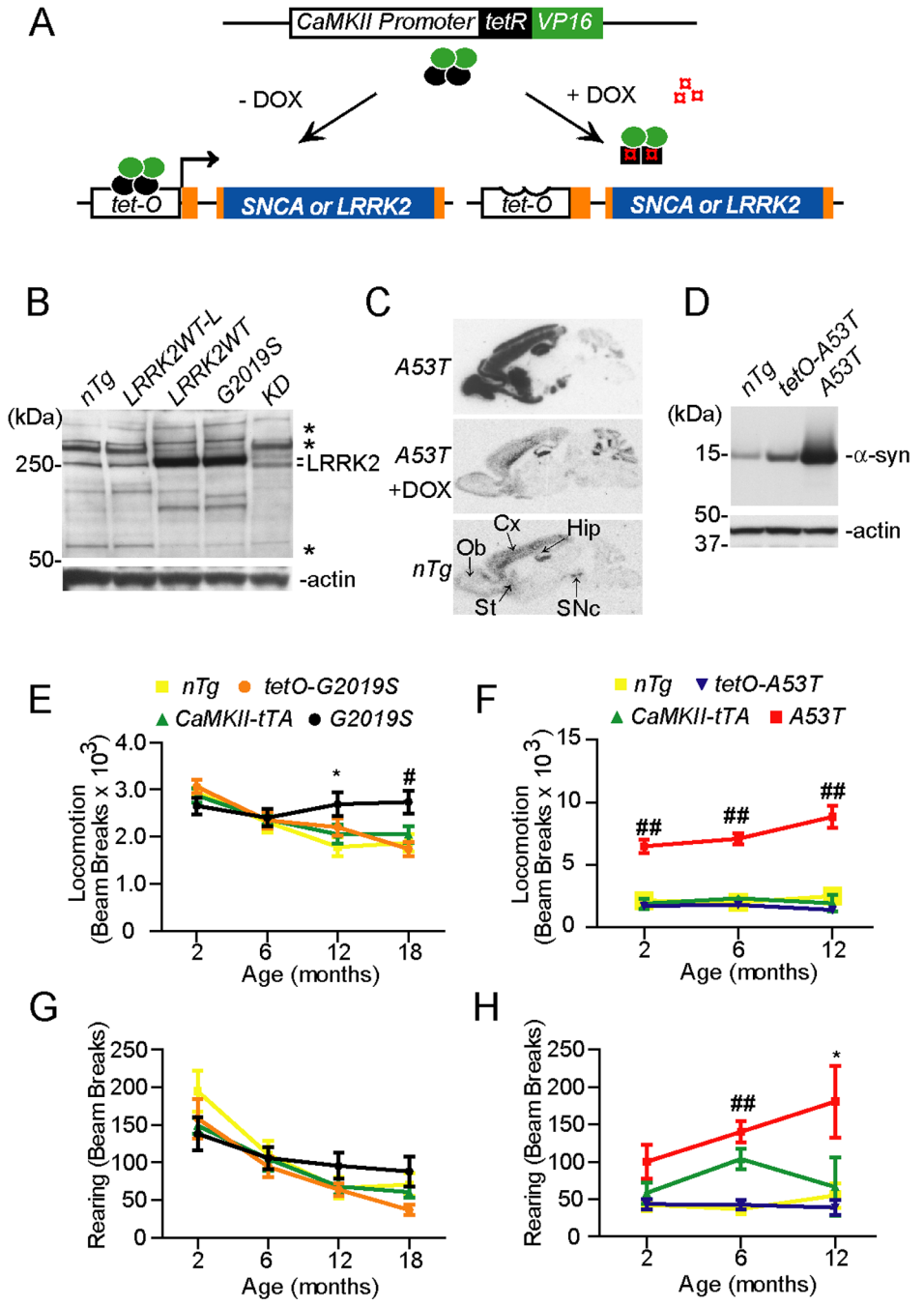

Figure 1. Generation and behavioral characterization of *LRRK2* and*α-syn* inducible transgenic mice

(A) The schematic diagram shows the generation of α-*syn* and *LRRK2* inducible transgenic mice using the “tet off” system.

(B) Western blot analysis shows LRRK2 expression in the brain of *nTg*, *LRRK2WT-L*, *LRRK2WT*, *G2019S*, and *KD* transgenic mice using a LRRK2 C-terminal antibody. Asterisks marked non-specific bands. LRRK2 appeared as doublet in *KD* sample.

(C) The expression pattern of *A53T* α-*syn* transgene in the brain by *in situ* hybridization using a P^{33}-labeled human/mouse α-syn-specific oligo probe (upper panel). The expression of transgenic α-syn was suppressed by administering the animals with doxycycline (DOX)-

containing feed for 4 wks (middle panel). The endogenous α-syn was also highly expressed by SNpc DA neurons (bottom panel). Ob: olfactory bulb; Cx: cortex; St: Striatum; Hip: hippocampus; SNpc: substantia nigra pars compacta.

(D) Western blots of α-syn expression in the brain of *nTg*, *tetO-A53T*, and *A53T* transgenic mice using an antibody recognizing both mouse and human α-syn.

(E, G) The *nTg* (n = 10), *tetO-G2019S* (n = 10), *CaMKII-tTA* (n = 14), and *G2019S* (n = 12) mice were subjected to Open-field tests. The ambulatory (E) and rearing activities (G) were quantified in the Open-field test. *$p<0.05$, $^{\#}p<0.005$

(F, H) *A53T* transgenic and control mice were subjected to Open-field test to evaluate their ambulatory (F) and rearing (H) activities. n =10 per genotype. *$p<0.05$, $^{\#\#}p<0.001$

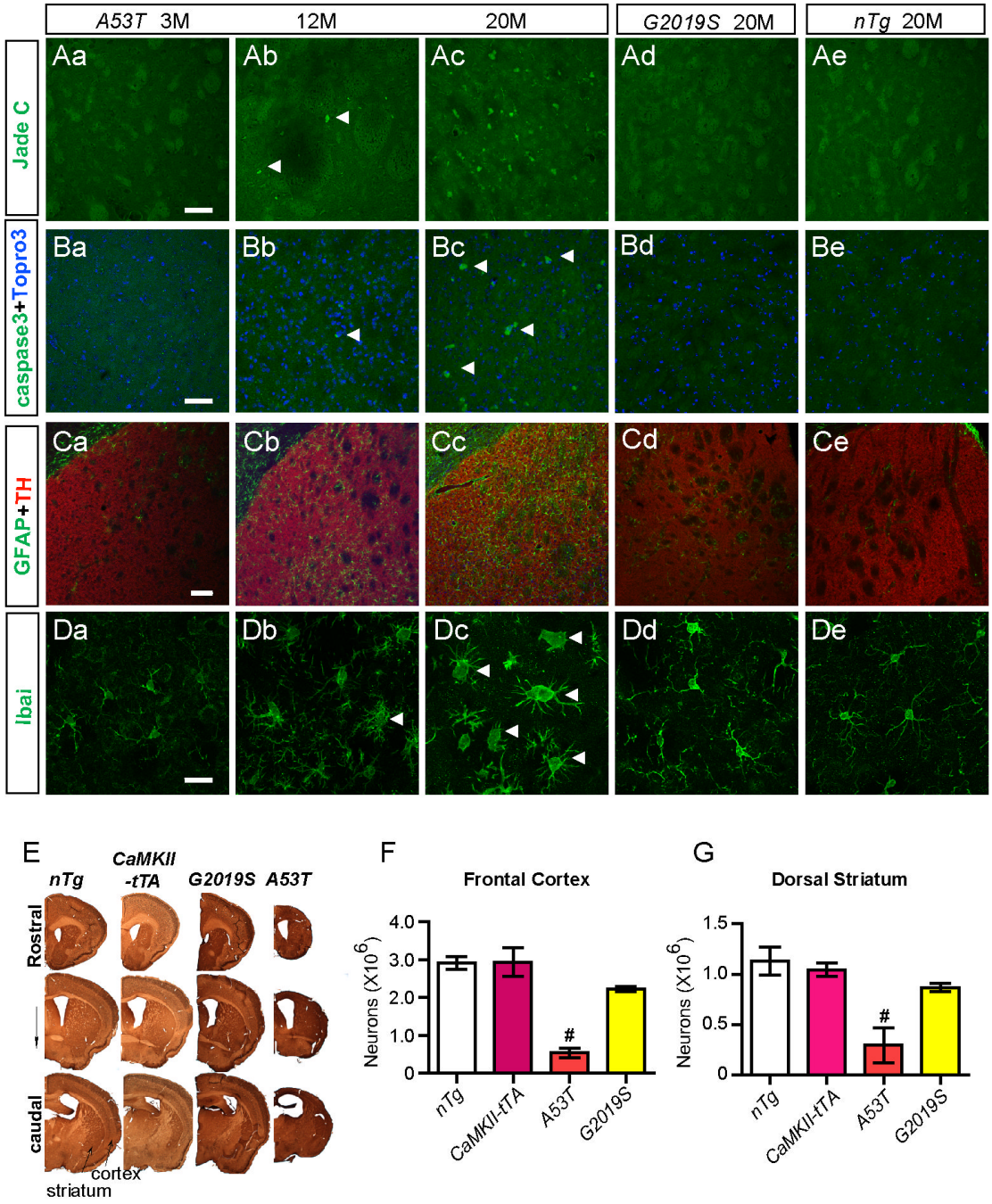

Figure 2. *A53T* but not *G2019S* transgenic mice develop progressive neuropathology

(Aa–Ae) Representative images show Jade C staining (arrowheads) in the striatum of *A53T* mice at 3 (a), 12 (b), and 20 (c) months of age, and of *G2019S* (d) and control *nTg* (e) mice at 20 months of age. Scale bar: 50 μm

(Ba–Be) Representative images show cleaved-caspase 3 (caspase3) staining (white arrowheads) in the striatum of *A53T* mice at 3 (a), 12 (b), and 20 (c) months of age, and of *G2019S* (d) and control *nTg* (e) mice at 20 months of age. Nuclei were stained with Topro 3 (blue). Scale bar: 50 μm

(Ca–Ce) Representative images reveal GFAP staining (green) in the striatum of *A53T* mice at 3 (a), 12 (b), and 20 (c) months of age, and of *G2019S* (d) and control *nTg* (e) mice at 20 months

of age. The section was counter-stained with an antibody against tyrosine hydroxylase (TH) (red). Scale bar: 100 μm

(Da–De) Representative images show Iba1 staining (green) in the striatum of *A53T* mice at 3 (a), 12 (b), and 20 (c) months of age, and of *G2019S* (d) and control *nTg* (e) mice at 20 months of age. Scale bar: 20 μm

(E) Representative images display coronal sections co-stained with NeuN and TH across the striatum of 20-month old *nTg*, *CaMKII-tTA*, *G2019S*, and *A53T* mice.

(F–G) Bar graphs depict the numbers of neurons remained the frontal cortex (F) and dorsal striatum (G) of 20-month old *nTg*, *CaMKII-tTA*, *G2019S*, and *A53T* mice. $^{\#}p < 0.005$ *vs. nTg*

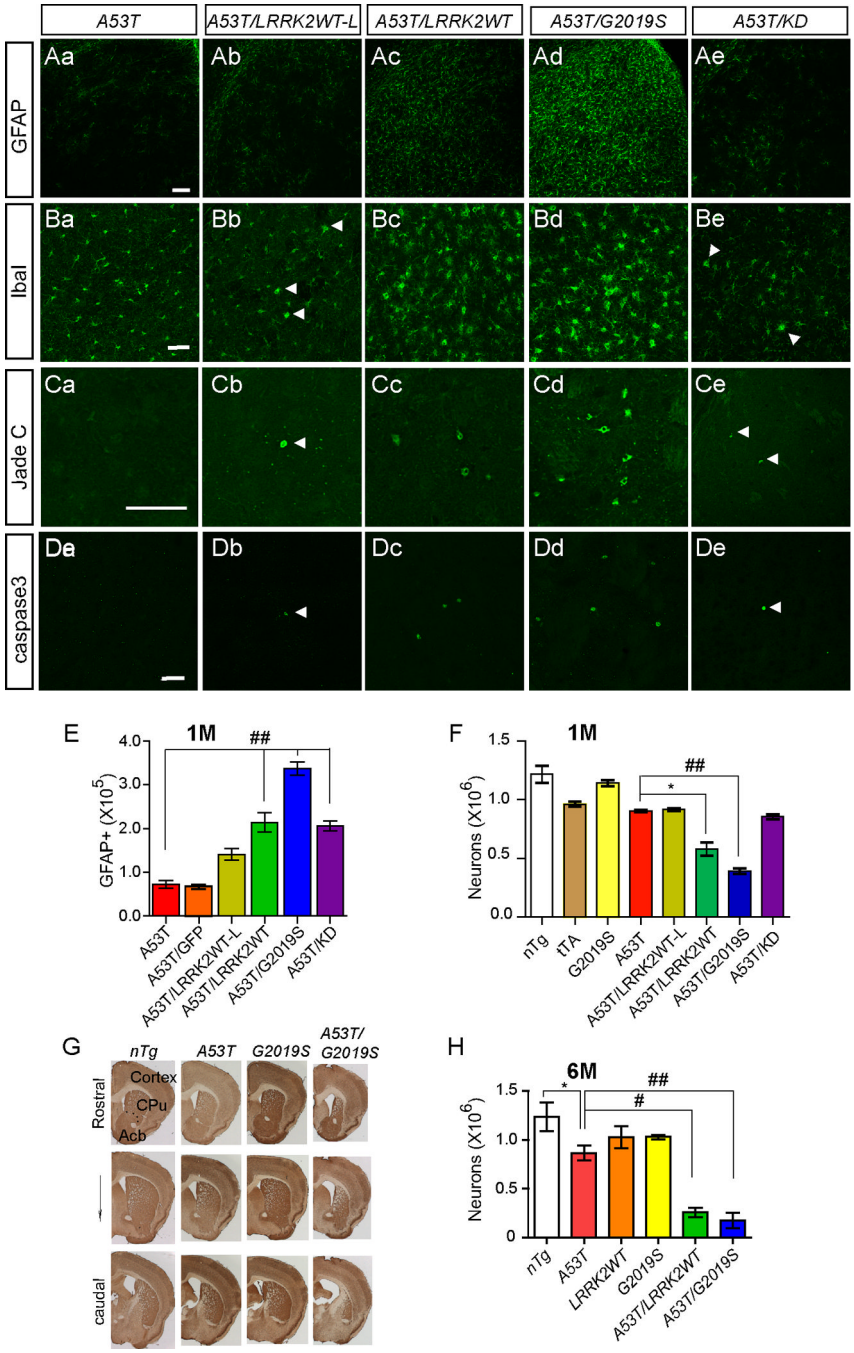

Figure 3. *LRRK2* accelerates the progression of A53 α-syn-mediated neuropathology

(Aa–Ae) Representative images show GFAP staining in the striatum of 1-month old *A53T* (a), *A53T/LRRK2WT-L* (b), *A53T/LRRK2WT* (c), *A53T/G2019S* (d), and *A53T/KD* (e) mice. Scale bar: 100 μm

(Ba–Be) Representative images show Iba1 staining in the striatum of 1-month old *A53T* (a), *A53T/LRRK2WT-L* (b), *A53T/LRRK2WT* (c), *A53T/G2019S* (d), and *A53T/KD* (e) mice. Scale bar: 50 μm

(Ca–Ce) Representative images show Jade C staining in the striatum of 1-month old *A53T* (a), *A53T/LRRK2WT-L* (b), *A53T/LRRK2WT* (c), *A53T/G2019S* (d), and *A53T/KD* (e) mice. Scale bar: 20 μm

(Da–De) Representative images show caspase3 staining in the striatum of 1-month old *A53T* (a), *A53T/LRRK2WT-L* (b), *A53T/LRRK2WT* (c), *A53T/G2019S* (d), and *A53T/KD* (e) mice. Scale bar: 50 μm

(E–F) Bar graphs reveal the numbers of GFAP-positive ($GFAP^+$, E) and NeuN-positive cells (F) in the dorsal striatum estimated by unbiased stereological methods. *$p < 0.05$, $^{\#\#}p < 0.001$

(G) Representative images show coronal sections across the striatum of 6-month old *nTg, A53T, G2019S, A53T/G2019S* mice. The section was co-stained with NeuN and TH.

(H) Bar graph depicts the numbers of neurons remained the dorsal striatum (G) of 6-month old *nTg, A53T, LRRK2WT, G2019S, A53T/LRRK2WT* and *A53T/G2019S* mice. *$p < 0.05$, $^{\#}p < 0.005$, $^{\#\#}p < 0.001$

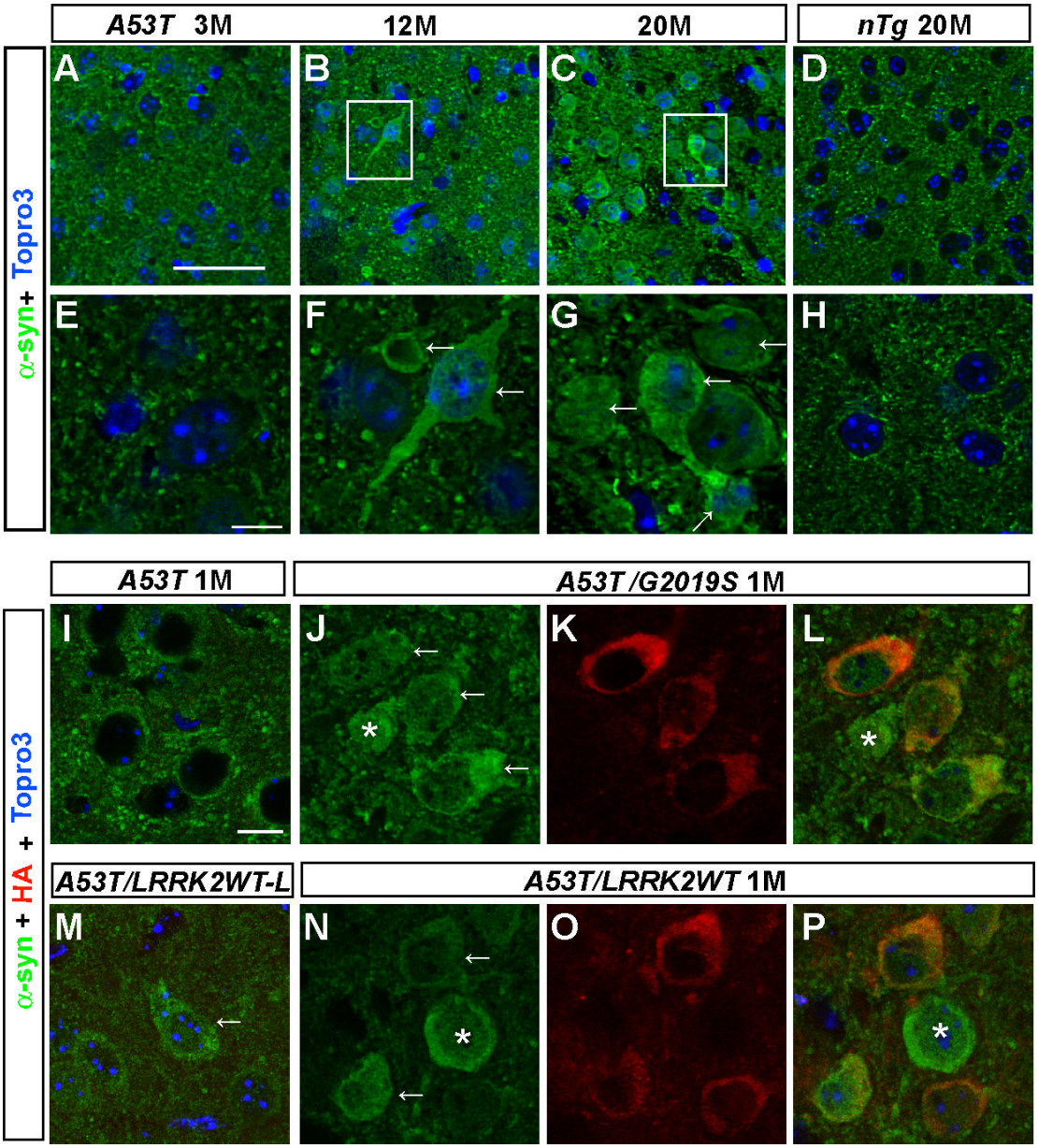

Figure 4. *LRRK2* accelerates somatic accumulation of A53T α-syn in neurons

(A–H) Representative images show α-syn staining (green) in striatal neurons of *A53T* mice at 3 (A), 12 (B), and 20 months of age (C), and *nTg* mice at 20 months of age (D). F and G represent enlarged images with the white boxes in B and C. Nuclei were stained with Topro 3 (blue). Scale bars: 50 μm (A–D); 10 μm (E–H).

(I–P) Representative images reveal α-syn staining (green) in striatal neurons of 1-month old *A53T* (I), *A53T/G2019S* (J, L), *A53T/LRRK2WT-L* (M), and *A53T/LRRK2WT* (N, P) mice. Human LRRK2 was stained with an anti-HA antibody (red, K–L, O–P). Nuclei were stained with Topro 3 (blue). Scale bar: 10 μm.

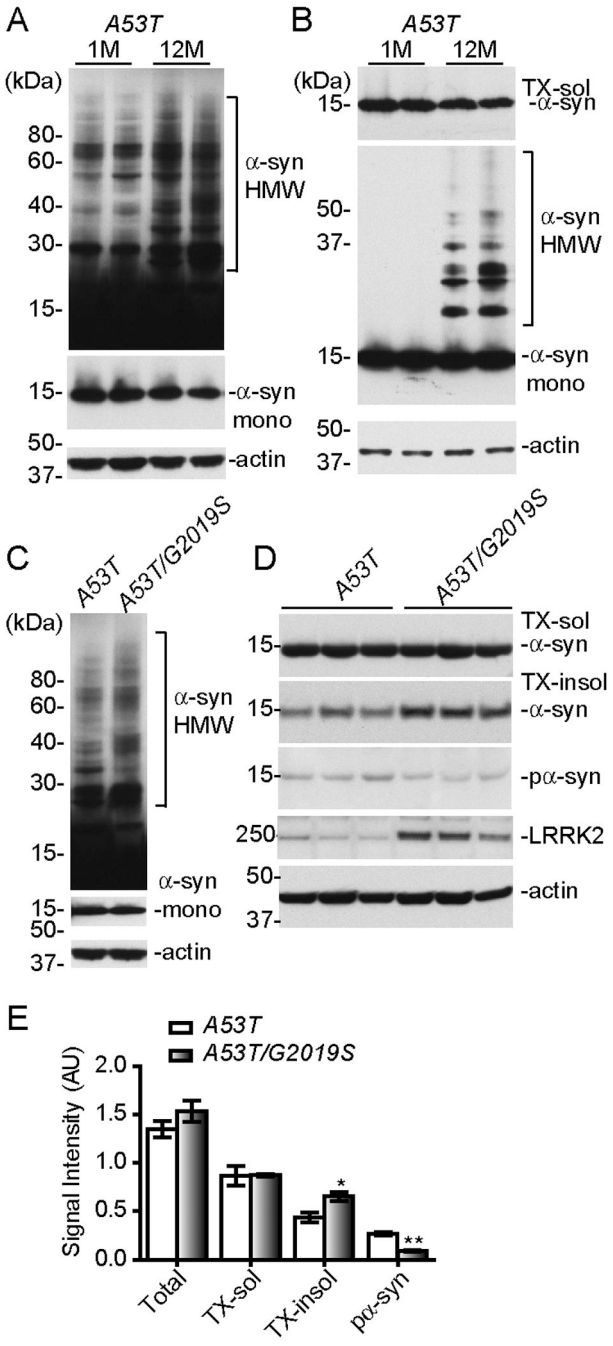

Figure 5. *LRRK2* promotes the formation of α-syn Aggregates

(A–B) Western blots show high molecular weight (HMW) bands of α-syn in the total (A) and sequentially detergent-extracted (B) brain homogenates of *A53T* transgenic mice at 1 and 12 months of age. The middle panel in (A) shows the monomeric α-syn (α-syn mono) under lower exposure.

(C) Western blots show α-syn-positive HMW bands in the total brain homogenates of *A53T* single and *A53T/G2019S* double transgenic mice at 1 month of age. The middle panel in (C) shows the monomeric α-syn with shorter exposure.

(D) Western blots show phosphorylated α-syn (pα-syn) in the total and monomeric α-syn in sequentially detergent-extracted fractions of brain homogenates of *A53T* single and *A53T/G2019S* double transgenic mice at 1 month of age.
(E–F) Bar graphs compare the levels of α-syn and pα-syn in different fractions of brain homogenates (E) of *A53T* and *A53T/G2019S* transgenic mice at 1 month of age. *$p<0.05$, **$p<0.01$

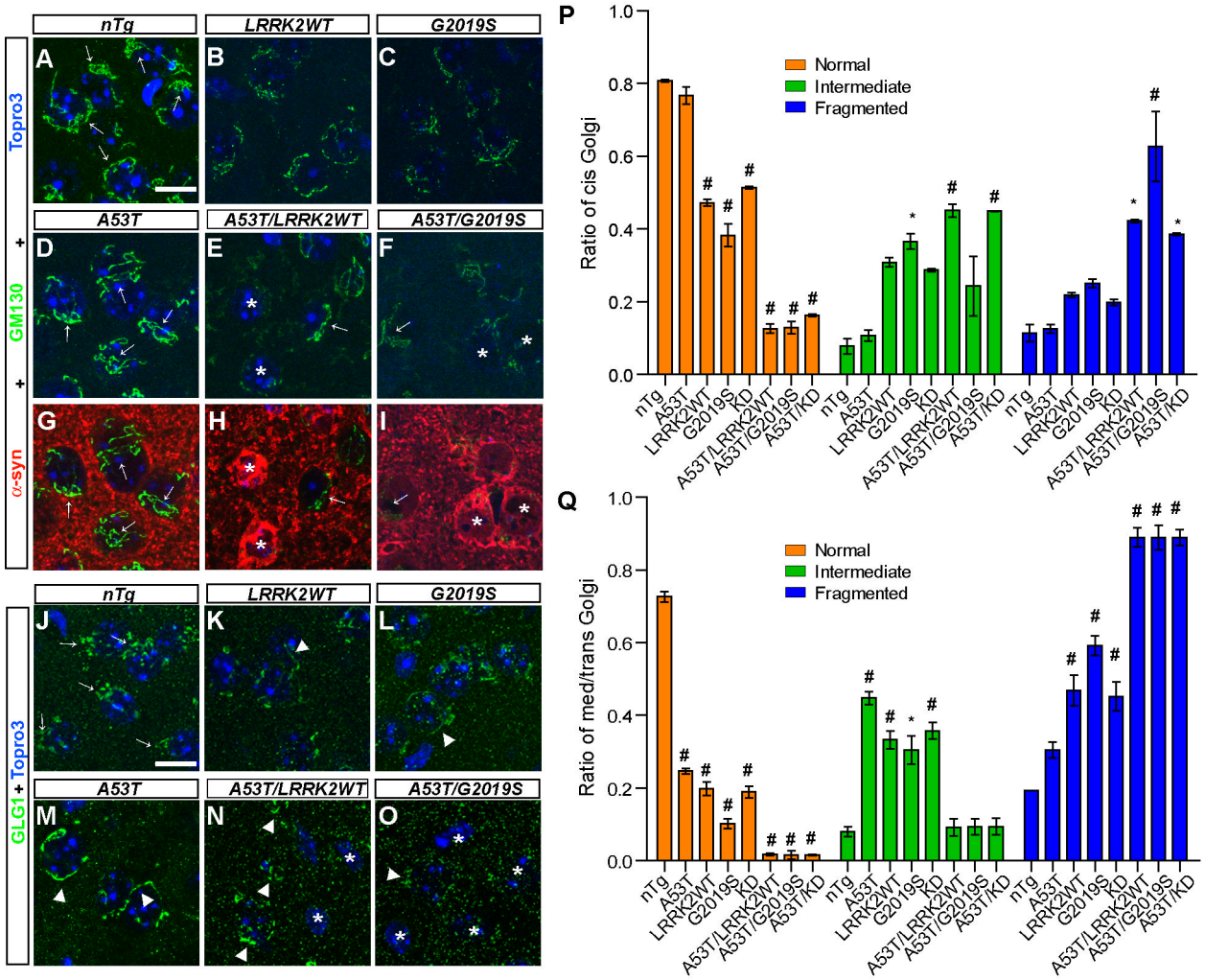

Figure 6. α-syn and LRRK2 cause synergistic damage to Golgi apparatus

(A–I) Representative images show GM130 staining (arrows, green) in the striatum of *nTg* (A), *LRRK2WT* (B), *G2019S* (C), *A53T* (D, G), *A53T/LRRK2WT* (E, H) and *A53T/G2019S* (F, I) mice at 1 month of age. Co-staining of GM130 (green) and α-syn (red) was shown in the striatum of *A53T* (G), *A53T/LRRK2WT* (H) and *A53T/G2019S* (I) mice. Neurons displaying somatic accumulation of α-syn were marked with asterisks. Normal GM130 staining was pointed by arrows in neurons. Nuclei were labeled by Topro 3 staining (blue). Scale bar: 10 μm

(J–O) Representative images show GLG1 staining (green) in the striatum of *nTg* (J), *LRRK2WT* (K), *G2019S* (L), *A53T* (M), *A53T/LRRK2WT* (N) and *A53T/G2019S* (O) mice at 1 month of age. Normal GLG1 staining was pointed by arrows in neurons; and abnormal tubular and fragmented GLG1 staining was marked by arrowheads. Neurons with complete fragmentation of Golgi were marked with asterisk. Nuclei were labeled by Topro 3 staining (blue). Scale bar: 10 μm.

(P–Q) Bar graphs quantify the morphological changes of cis- (P) and trans- (Q) Golgi in neurons (> 300 neurons and ≥ 3 mice per genotype). *$p < 0.05$, #$p < 0.0005$

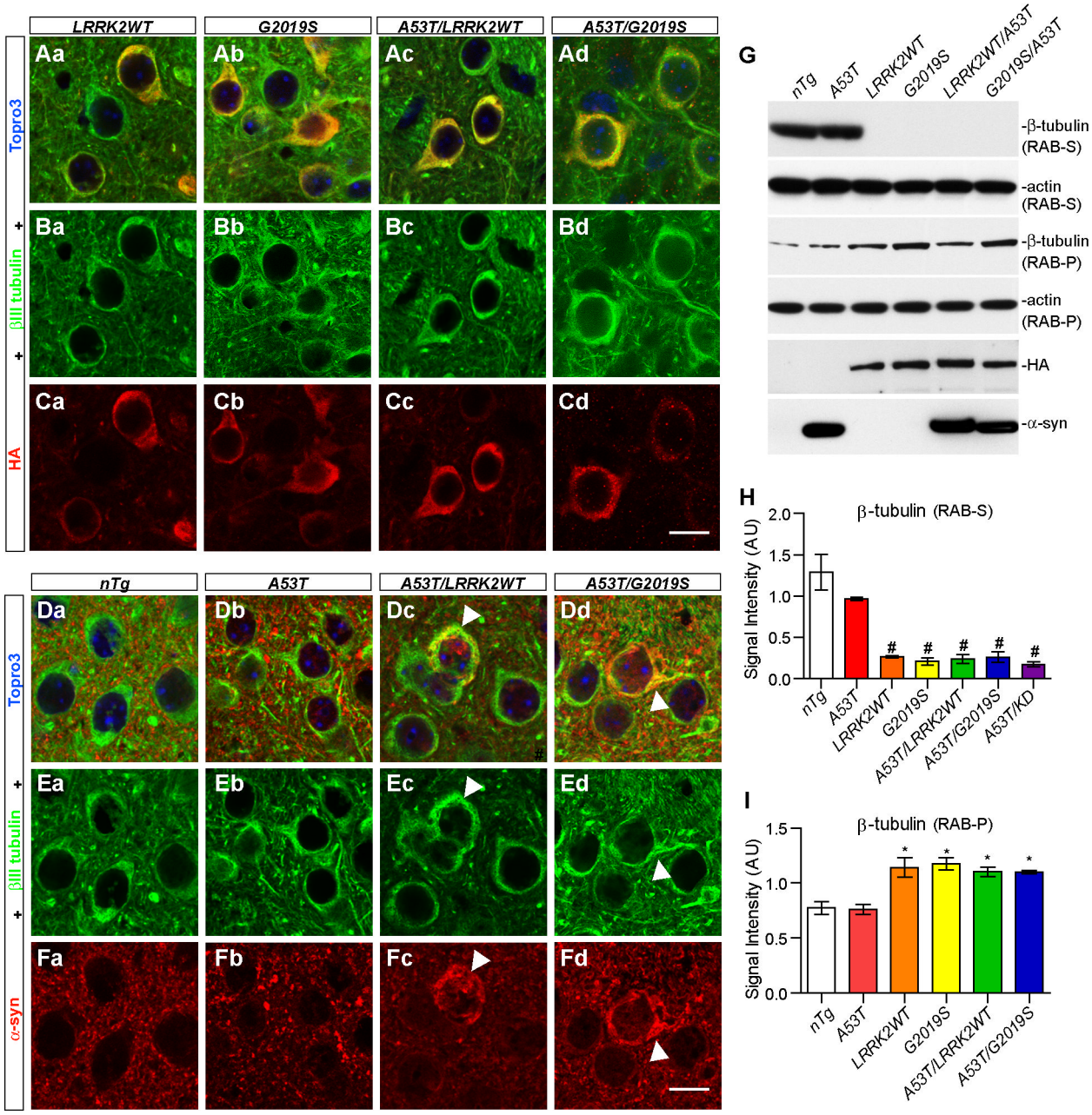

Figure 7. Over-expression of *LRRK2* impairs the dynamics of microtubules

(A–C) Representative images show βIII tubulin (green) and HA (red) staining in the striatum of *LRRK2WT* (Aa, Ba, and Ca), *G2019S* (Ab, Bb, and Cb), *A53T/LRRK2WT* (Ac, Bc, and Cc) and *A53T/G2019S* (Ad, Bd, and Cd) mice at 1 month of age. Nuclei were labeled by Topro 3 staining (blue). Scale bar: 10 μm.

(D–F) Representative images show βIII tubulin (green) and α-syn (red) staining in the striatum of *nTg* (Da, Ea, and Fa), *A53T* (Db, Eb, and Fb), *A53T/LRRK2WT* (Dc, Ec, and Fc) and *A53T/G2019S* (Dd, Ed, and Fd) mice at 1 month of age. The abnormal somatic accumulation of α-syn and βIII tubulin was marked by arrowheads. Nuclei were labeled by Topro 3 staining (blue). Scale bar: 10 μm.

(G) Western blots of β-tubulin in RAB buffer-soluble supernatant (RAB-S) and insoluble pellet (RAB-P) fractions of brain homogenates from various transgenic mice at 1 month of age and age-matched *nTg* controls.

(H–I) Bar graphs quantify the levels of β- tubulin in RAB-S (H) and RAB-P (I) fractions of brain homogenates of transgenic mice at 1 month of age and age-matched *nTg* controls. *$p < 0.05$, $^{\#\#}p < 0.001$

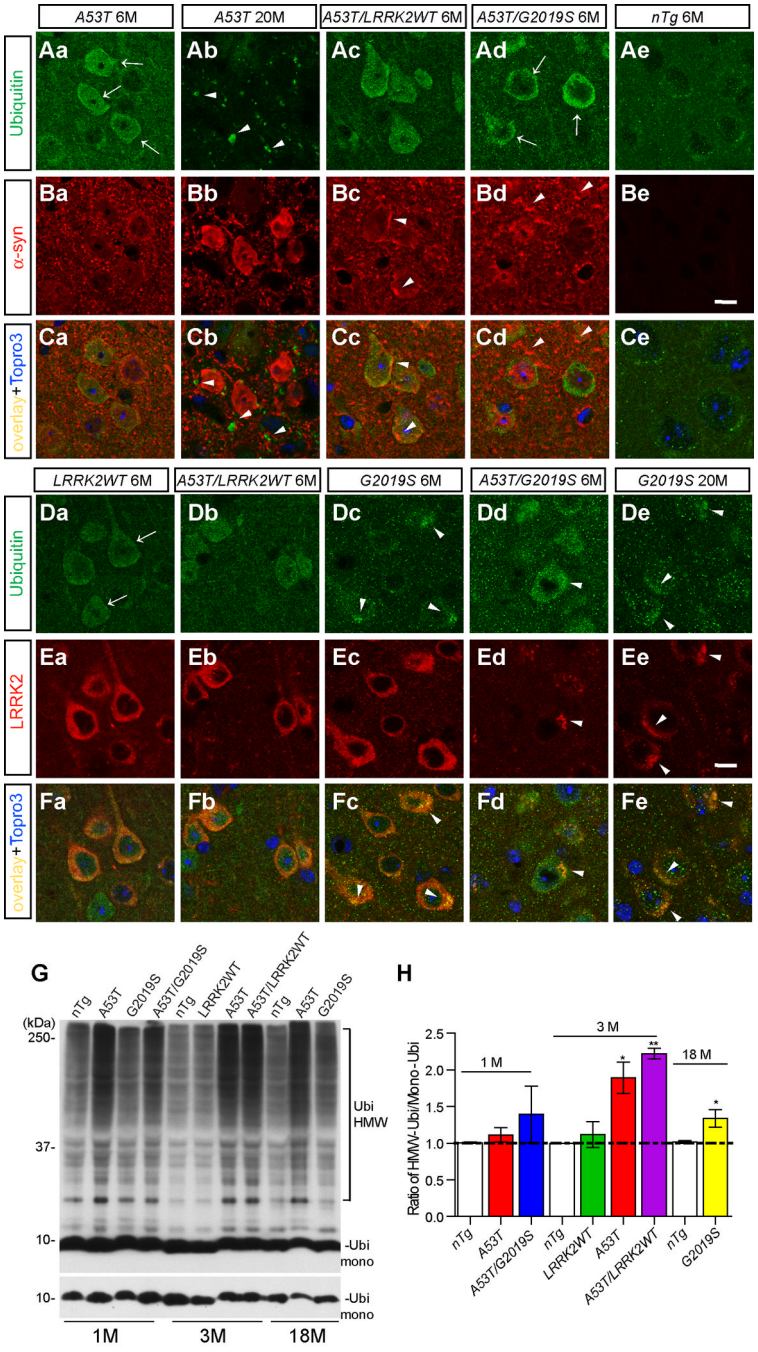

Figure 8. Over-expression of *A53T* and *LRRK2* impairs the UPS activities in neurons

(A–C) Representative images show Ubi staining (arrows, green) in the cortex of *A53T* mice at 6 (Aa) and 20 (Ab) months of age, and *A53T/LRRK2WT* (Ac), *A53T/G2019S* (Ad), and *nTg* (Ae) mice at 6 months of age. Images from Ba to Be display corresponding α-syn staining (red); while images from Ca to Ce show the overlay of Ubi and α-syn staining. Nuclei were labeled by Topro 3 staining (blue). Scale bar: 10 μm

(D–F) Representative images show Ubi staining (arrows, green) in the cortex of *LRRK2WT* (Da) and *A53T/LRRK2WT* (Db) mice at 6 months of age; *G2019S* (Dc) and *A53T/G2019S* (Dd) mice at 6 and *G2019S* mice at 20 (De) months of age. Images from Ea to Ee display

corresponding LRRK2 staining (red); whilst images from Fa to Fe show the overlay of Ubi and LRRK2 staining. Nuclei were labeled by Topro 3 staining (blue).
(G) Western blots show Ubi-positive HMW bands in the total brain homogenates of *nTg*, *A53T*, *G2019S*, and *A53T/G2019S* mice at 1 month of age; *nTg*, *LRRK2WT*, *A53T*, and *A53T/LRRK2WT* mice at 3 months of age; and *nTg*, *A53T*, and *G2019S* mice at 18 months of age. The bottom panel in (G) shows the level of monomeric Ubi (Ubi mono) with shorter exposure.
(H) Bar graph shows the ratio of HMW/mono-Ubi in the total brain homogenates of mice with different genotype at 1, 3, 18 months of age. *$p<0.05$, **$p<0.01$

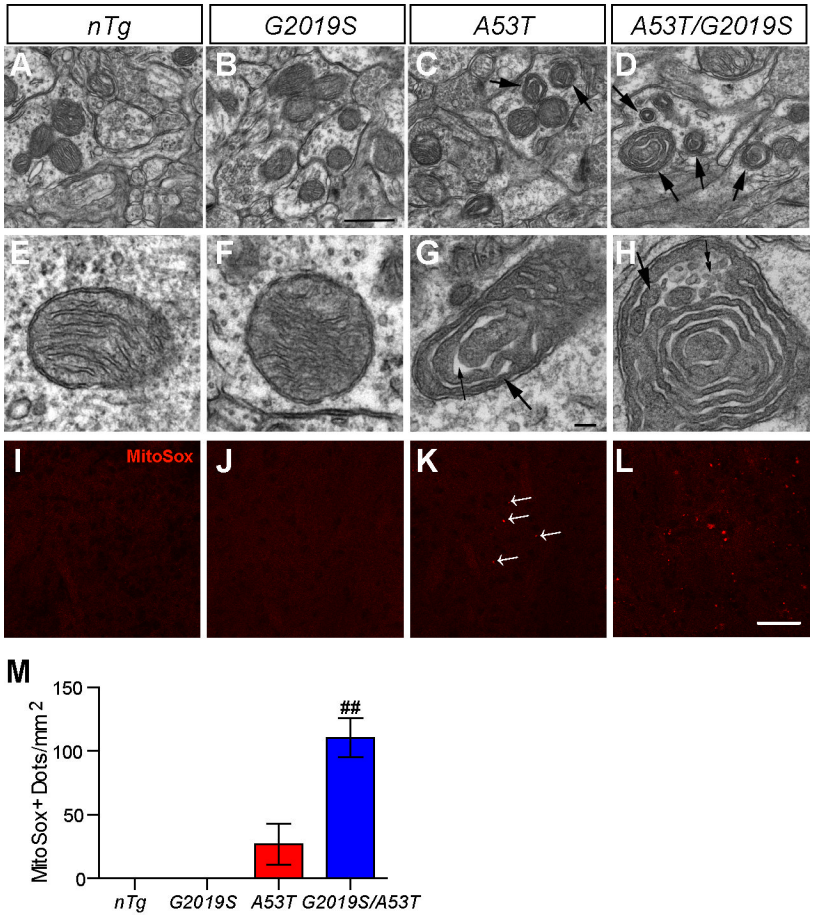

Figure 9. *LRRK2* exacerbates α-syn-induced mitochondrial structural and functional abnormalities

(A–H) Representative EM images show mitochondria in the striatum of *nTg* (A, E), *G2019S* (B, F), *A53T* (C, G), and *A53T/G2019S* (D, H) transgenic mice at 1 month of age. The abnormal mitochondria were marked by arrows (C, D). The dense matrix of the abnormal mitochondria in G and H often appear "sausage-like" with multiple constrictions (large arrows in G, H) and concentric in arrangement, and occasionally became vesiculated (small double arrows in H). N = 2 per genotype. Scale bar: 0.5 μm (A–D); 0.1 μm (E–H). (I–L) Representative images show the MitoSox Red staining in the striatum of *nTg* (I), *G2019S* (J), *A53T* (K), and *A53T/G2019S* (L) mice at 1 month of age. Scale bar: 50 μm. (M) Bar graph shows the quantification of MitoSox Red staining shown in I–L. $^{\#\#}p < 0.001$

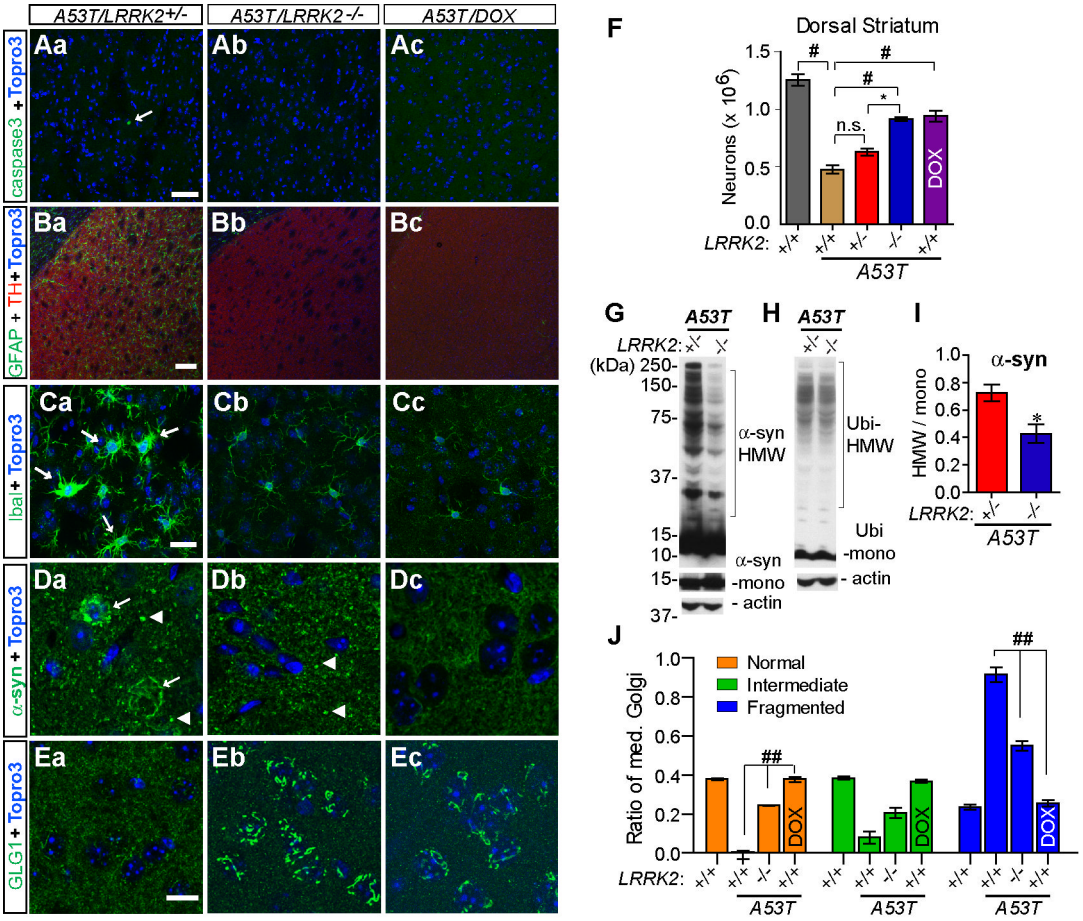

Figure 10. Inhibition of *LRRK2* delays the progression of A53T α-syn-mediated neuropathology and reduces the somatic accumulation and aggregation of α-syn

(Aa–Ec) Representative images show caspase3 (Aa–Ac), GFAP (Ba–Bc), Iba1 (Ca–Cc), α-syn (Da–Dc), and GLG1 (Ea–Ec) staining in the striatum of *A53T/LRRK2*$^{+/-}$ and littermate *A53T/LRRK2*$^{-/-}$ mice, and *A53T/DOX* mice at 12 months of age. The caspase3-positive neuron (Aa), activated microglia (Ca) and somatic accumulation of α-syn (Da) were pointed by arrows. The enlarged and α-syn-positive nerve terminals were labeled with arrowhead (Da and Db). The striatum was outlined by TH staining (red, Ba–Bc). Nuclei were labeled by Topro 3 staining (blue). Scale bar: 100 μm (Ba–Bc), 50 μm (Aa–Ac), 20 μm (Ca–Cc), 10 μm (Da–Ec).

(F) Bar graph depicts the numbers of neurons remained the dorsal striatum of 12-month old *LRRK2*$^{+/+}$, *A53T/LRRK2*$^{+/+}$, *A53T/LRRK*$^{+/-}$, *A53T/LRRK2*$^{-/-}$, and *A53T/DOX* mice. *$p < 0.05$, $^{\#}p < 0.001$

(G–H) Western blots show HMW α-syn (G) and Ubi-positive bands (H) in the total homogenates from 12 month-old *A53T/LRRK2*$^{+/-}$ and *A53T/LRRK2*$^{-/-}$ mice.

(I) Densitometry analyses revealed significant reduction of HMW α-syn in the brain homogenates of 12-month old *A53T/LRRK2*$^{-/-}$ mice (n=3) compared to age-matched *A53T/LRRK*$^{+/-}$ mice (n= 4). *$p < 0.05$

(J) Quantification of trans-Golgi morphology in striatal neurons (≥ 300 per genotype) of mutant and control mice (≥ 3 per genotype) at 12 months of age. $^{\#\#}p < 0.0001$

Table 1

Neuronal degeneration in the striatum and cortex of*A53T* and *LRRK2* mutant mice

Age	*Genotype*	*# of c. caspase 3*$^+$ Striatum	Cortex	*# of Jade C*$^+$ Striatum	Cortex
1M	*nTg*	0	0	0	0
	tTA	0	0	0	0
	A53T	0	0	0	0
	LRRK2WT-L	0	0	0	0
	LRRK2WT	0	0	0	0
	KD	0	0	0	0
	G2019S	0	0	0	0
	A53T/LRRK2WT-L	1.4±0.2	2.4±0.2	3.4±0.5	5.2±0.5[f]
	A53T/LRRK2WT	3.0±0.7	8.0±1.1	12.0±0.9[b]	15.8±1.1[b]
	A53T/G2019S	13.0±1.5[b,c]	17.3±0.3	26.0±1.2[b]	28.7±1.9[b]
	A53T/KD	1.3±0.3	3.0±0.1	2.7±0.3	8.0±1.3[e]
12M	*nTg (DOX)*	0	0	0	0
	A53T	5.0±0.6	6.3±0.5	12.0±0.6	13.3±1.5
	A53T/LRR2$^{-/-}$	0	0	0	0
	A53T (DOX)	0	0	0	0
	LRRK2WT	0	0	0	0
20M	*nTg**	0	0	0	0
	A53T	24.7±4.1	32±4.4	33.3±4.1	40.3±4.3
	G2019S	0	0	0	0
	LRRK2$^{-/-}$	0	0	0	0

The average numbers of c. caspase 3$^+$ and Jade C$^+$ cells in the striatum and cortex of each cohort of mice were counted by the event measurement tool of AxioVision (Zeiss). Two matched sections were analyzed for each mouse and three or more animals per genotype were used for each age group. The randomly selected sampling area was ~140, 000 μm^2 per brain region for each animal. *nTg** represents *nTg* mice from both transgenic and *LRRK2*$^{-/-}$ cohorts of mice. At 1 month of age, significantly more cleaved caspase 3 positive (c. caspase3$^+$) neurons were revealed in the striatum and cortex of *A53T/G2019S* mice as compared to that of *A53T* (b, $p < 0.0005$) and *A53T/LRRK2WT* mice (c, $p < 0.005$). Additionally, more Jade C positive (Jade C$^+$) cells were found in the striatum and cortex of *A53T/LRRK2WT-L, A53T/LRRK2WT, A53T/KD* and *A53T/G2019S* mice as compared to that of *A53T* mice (b, $p < 0.0005$; e, $p < 0.01$; f, $p < 0.05$). More Jade C+ cells were also detected in the striatum and cortex of *A53T/G2019S* mice as compared to that of *A53T/LRRK2WT* mice (b, $p < 0.0005$).

Table 2

Activation of microglia in the striatum of *A53T* and *LRRK2* mutant mice

Age	*Genotype*	*Ratio (%)*	Size (μm^2)
1M	*nTg*	0	31.77±0.46
	tTA	0	28.95±1.63
	A53T	0	36.83±0.86
	G2019S	0	31.69±0.76
	A53T/LRRK2WT-L	5.88	44.40±3.73
	A53T/LRRK2WT	31.64	52.01±1.60[a]
	A53T/G2019S	83.10	79.55±7.01[b]
	A53T/KD	11.11	46.66±0.05
12M	*nTg (DOX)*	0	38.52±0.01[c]
	A53T	38.71	60.97±2.46
	A53T/LRRK2$^{-/-}$	0	29.93±2.90[d]
	A53T (DOX)	0	36.91±0.06[c]
20M	*nTg**	0	31.44±1.17
	A53T	79.63	102.07±10.88[e,f]
	G2019S	0	33.33±0.63
	LRRK2$^{-/-}$	11.11	45.00±2.32[f]

The numbers of total and activated Iba1$^+$ cells in the striatum were counted by the event measurement tool of AxioVision. The ratio of activated Iba1$^+$ cells were calculated by dividing the number of enlarged Iba1$^+$ cells with the total number of Iba1$^+$ cells. The size of Iba1$^+$ cell bodies were assessed by the outline function of AxioVision. Two matched sections were analyzed for each mouse and three or more animals per genotype were used for each age group. The area of sampled striatum was ~140, 000 μm^2 for each animal. At 1 month of age, enlarged Iba1$^+$ cells were only detected in *A53T* and *LRRK2* double transgenic mice. While the average size of Iba1$^+$ cell bodies appears larger in *A53T* and *LRRK2* double transgenic mice, it reached statistically significance in only *A53T/LRRK2WT* and *A53T/G2019S* mice as compared to *A53T* mice (a, $p < 0.02$; b, $p < 0.0005$). At 12 months of age, more enlarged Iba1$^+$ cells were detected in *A53T* with increasing size of cell bodies. In contrast, no apparent enlargement of Iba1$^+$ cells was found in *nTg*, *A53T/LRKK2*$^{-/-}$, or *A53T (DOX)* mice as compared to *A53T* mice (c, $p < 0.005$; d, $p < 0.002$). At 20 months of age, more and larger enlarged Iba1$^+$ cells were found in *A53T* mice as compared to *nTg* and *G2019S* mice (e, $p < 0.01$), and 12-month old *A53T* mice (f, $p < 0.05$). Interestingly, more enlarged Iba1$^+$ cells were detected in *LRRK2*$^{-/-}$ mice as compared to *nTg* mice (f, $p < 0.05$). *nTg** represents *nTg* mice from both transgenic and *LRRK2*$^{-/-}$ cohorts of mice.

Table 3

The prevalence of somatic accumulation of α-syn in the striatal neuron of *A53T* transgenic mice

Age	Genotype	Ratio (%)
1M	*nTg*	0
	tTA	0
	A53T	1.00
	G2019S	0
	A53T/LRRK2WT-L	6.19
	A53T/LRRK2WT	17.94[d]
	A53T/G2019S	30.36[b]
	A53T/KD	10.59[a]
12M	*nTg*	0
	A53T	23.48
	A53T/LRRK2$^{-/-}$	2.13[f]
	A53T (DOX)	0.69[a]
20M	*nTg**	0
	A53T	76.99
	G2019S	0
	LRRK2$^{-/-}$	0

The ratio of striatal neurons displaying apparent somatic accumulation of α-syn was calculated from each cohort of mice. Two matched sections were analyzed for each mouse and three or more animals per genotype were used for each age group. The area of sampled striatum was ~140, 000 μm^2 for each animal. *nTg** represents *nTg* mice from both transgenic and *LRRK2*$^{-/-}$ cohorts of mice. At 1 month of age, significantly more neurons with apparent somatic accumulation of α-syn were detected in the striatum of *A53T/LRRK2WT*, *A53T/G2019S*, and *A53T/KD* mice as compared to *A53T* mice (a, $p < 0.02$; b, $p < 0.0005$; and d, $p < 0.001$). At 12 months of age, less neurons with somatic accumulation of α-syn was found in the striatum of *A53T/LRKK2*$^{-/-}$ and *A53T (DOX)* mice as compared to *A53T* mice (a, $p < 0.02$; f, $p < 0.05$).